



Computer-aided diagnosis of diabetic retinopathy: A review



Muthu Rama Krishnan Mookiah ^{a,*}, U. Rajendra Acharya ^{a,b}, Chua Kuang Chua ^a, Choo Min Lim ^a, E.Y.K. Ng ^c, Augustinus Laude ^d

^a Department of Electronics and Computer Engineering, Ngee Ann Polytechnic, Singapore 599489 Singapore

^b Department of Biomedical Engineering, Faculty of Engineering, University of Malaya, 50603, Malaysia

^c School of Mechanical and Aerospace Engineering, Nanyang Technological University, Singapore 639798, Singapore

^d National Healthcare Group Eye Institute, Tan Tock Seng Hospital, Singapore 308433, Singapore

ARTICLE INFO

Article history:

Received 24 April 2013

Accepted 4 October 2013

Keywords:

Retina

Retinopathy

Fundus imaging

Computer-aided diagnosis

Pattern classification

Image processing

ABSTRACT

Diabetes mellitus may cause alterations in the retinal microvasculature leading to diabetic retinopathy. Unchecked, advanced diabetic retinopathy may lead to blindness. It can be tedious and time consuming to decipher subtle morphological changes in optic disk, microaneurysms, hemorrhage, blood vessels, macula, and exudates through manual inspection of fundus images. A computer aided diagnosis system can significantly reduce the burden on the ophthalmologists and may alleviate the inter and intra observer variability. This review discusses the available methods of various retinal feature extractions and automated analysis.

© 2013 Elsevier Ltd. All rights reserved.

Contents

1. Introduction	2137
1.1. Clinical features of DR	2137
1.2. Stages of diabetic retinopathy	2137
1.3. Diabetic retinopathy risk progression, complications and treatment	2137
1.4. Diabetic retinopathy screening systems	2138
2. Retinal imaging	2139
3. Detection and extraction of basic structures and clinical features	2139
3.1. Localization and segmentation of optic disk	2139
3.1.1. Optic disk localization	2139
3.1.2. Optic disk segmentation	2140
3.2. Segmentation of retinal vasculature	2141
3.3. Localization of the macula and fovea	2143
3.4. Segmentation of hard and soft exudates	2143
3.5. Segmentation of microaneurysms and hemorrhages	2145
3.6. Detection of macular edema	2147
4. Computer aided diagnosis of diabetic retinopathy	2148
5. Summary	2151
Conflict of interest statement	2151
Acknowledgments	2151
References	2151

* Corresponding author. Tel.: +65 64607889.

E-mail addresses: mkm2@np.edu.sg, mrk2k2@gmail.com (M.R.K. Mookiah).

1. Introduction

Diabetes mellitus (DM) is characterized by impaired metabolism of glucose caused by insulin deficiency or its resistance, leading to hyperglycemia which may finally result in vascular and neuropathic complications. DM is of two types: Type-1, caused by the destruction of autoimmune pancreatic β -cell and lack of insulin [1,2] and Type-2 diabetes caused by insulin resistance and relative lack of insulin. Insulin levels need to be monitored closely and failure of good glycaemic control may lead to organ damage, including Diabetic Retinopathy (DR). All diabetics may eventually develop DR [1].

The foremost risk factors of diabetes are increasing age, sedentary lifestyle and obesity [3]. The prevalence of diabetes population worldwide is expected to increase from 2.8% to 4.4% in the time span of 2000–2030 [3]. Nowadays, diabetes is identified among the people with age group of 30 years or even before. The incidence of DR is 50% after 10 years and 90% after 30 years of acquired diabetes. Usually DR does not develop within 5 years of the inception of diabetes or before puberty. About 5% of those with Type-2 diabetes have DR [4]. Uncontrolled diabetes and its complication leads to DR, which may result in loss of vision and blindness [4]. Patients with Proliferative Diabetic Retinopathy (PDR) are at increased risk of heart attack, stroke, diabetic nephropathy, amputation and death [4,5]. It was estimated that there were 171 million people in the world with diabetes in the year 2000 and this is projected to increase to 366 million by 2030 [6–8]. Early stages of DR may be clinically asymptomatic and the disease may be recognized in the advanced stage when treatment may become difficult [9]. Fig. 1 shows typical fundus images of normal, and different stages of DR.

1.1. Clinical features of DR

DR may cause several abnormalities in the retina, and are briefly explained below.

1. **Microaneurysms (MA)**—are the earliest visible sign of retinal damage. The abnormal permeability and/or non-perfusion of retinal blood vessels causes the formation of MA [10]. It is a red spot less than 125 μm in size and has sharp margins [11].

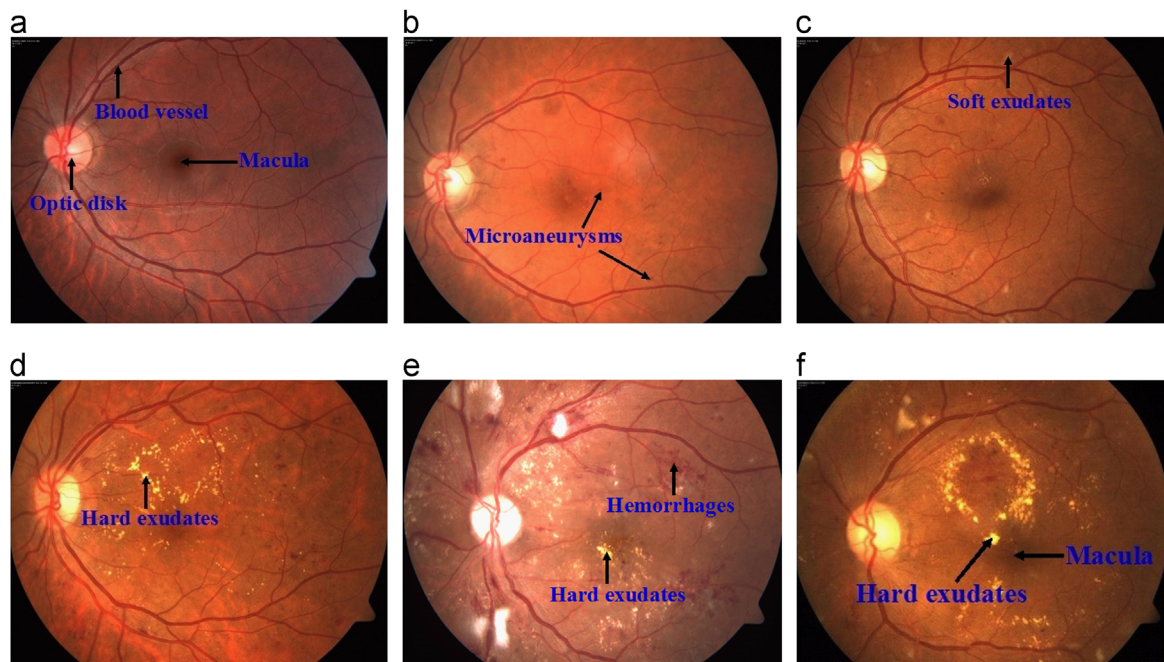


Fig. 1. Typical fundus images: (a) Normal; (b) Mild NPDR; (c) Moderate NPDR; (d) Severe NPDR; (e) Prolific DR; (f) Macular edema.

2. **Hard exudates**—are the lipoproteins and other proteins leaking through abnormal retinal vessels [1]. It appears as small white or yellowish-white deposits with sharp margins [11]. They are often arranged in clumps or circinate rings [4] and located in the outer layer of the retina [11].
3. **Soft exudates or Cotton Wool Spots (CWS)**—occur due to occlusion of arteriole [12]. The reduced blood flow to the retina causes ischemia of the Retinal Nerve Fibre Layer (RNFL) which affects the axoplasmic flow and causes accumulation of axoplasmic debris in the retinal ganglion cell axons. The debris accumulation appear as fluffy white lesions in the RNFL called as CWS [12,13].
4. **Hemorrhages (HEM)**—occur due to leakage of weak capillaries [1]. It is defined as a red spot with irregular margin and/or uneven density. Usually it is greater than 125 μm in size [11].
5. **Neovascularization (NV)**—is the abnormal growth of new blood vessels on the inner surface of the retina. These blood vessels are weak and frequently bleed into vitreous cavity, obscuring the vision [14,15].
6. **Macular edema (ME)**—is the swelling of the retina. It is caused due to permeability of abnormal retinal capillaries causing the leakage of fluid and solutes around the macula [10,16]. It affects the central vision [17,4].

1.2. Stages of diabetic retinopathy

Depending on the presence of clinical features, DR is classified into five types namely mild Non-Proliferative Diabetic Retinopathy (NPDR), moderate NPDR, severe NPDR, PDR and Macular Edema (ME) [11,18,1,19] which are briefly described in Table 1.

1.3. Diabetic retinopathy risk progression, complications and treatment

DR with MA has 6.2% possibility to develop into PDR within a year [20]. Increase in the number of MA is an important early feature of DR progression. The signs of pre-PDR includes venous loops, small vessel abnormality within retina and many blot HEM.

Table 1

Stages of DR [11,18,1,19].

Types of DR	Sub-types	Presence of clinical features
NPDR	Mild (see Fig. 1b)	MA, HEM, hard exudates and ME
	Moderate (see Fig. 1c)	<ul style="list-style-type: none"> • Widespread of HEM and \ or MA and \ or CWS • Venous Beading (VB) or Intra-Retinal Microvascular Abnormalities (IRMA)
	Severe (see Fig. 1d)	<p>MA, HEM, CWS, VB presents at least two quadrants of the retina. This can be defined using 4–2–1 rule.</p> <ul style="list-style-type: none"> • HEM in four quadrants • VB in two quadrants • Severe IRMA in one quadrant
PDR (see Fig. 1e)	Early PDR	Pre-retinal HEM
	High risk PDR	<ul style="list-style-type: none"> • Vitreous HEM • Neovascularisation on the disk • Neovascularisation anywhere on the disk • Retinal detachment • Neovascularisation of the iris
	Advanced PDR	
ME (see Fig. 1f)	Non-clinically significant ME	Presence of edema, retinal thickening or hard exudates, but not at or within 500 μm of the fovea
	Clinically significant ME	Presence of edema, retinal thickening or hard exudates on or within 500 μm of the fovea

With progression of ischemia, there is an increase in the possibility of PDR development within a year. This one year risk development rises from 11.3% to 54.8% from lower stage to advanced stage [20].

New blood vessels generally grow from venous and arterial circulation. Such patients have 25.6% to 36.9% [20] possibility of vision loss, if not treated properly. Moreover, PDR eyes not treated for more than 2 years have the possibility of 7.0% of visual loss and if it is not treated for more than 4 years have the possibility of 20.9% of visual loss. Vision loss decreases to 3.2% within 2 years of treatment and 7.4% within 4 years of treatment [20].

Patients with mild DR do not require any particular treatment other than optimal control of diabetes and the associated risk factors like hypertension, anaemia, renal failure. They need to be monitored closely, else it may progress to higher stages of DR. Recently, it was shown that pre-PDR can regress to background retinopathy with optimal diabetes control [4].

In the advanced stage of DR treatment is limited [21]. In severe neovascularization, several sessions of pan-retinal photocoagulation may be required to prevent visual loss from vitreous HEM and tractional retinal detachment. Inadequate laser treatment is one of the major causes of persistent neovascularization [21]. Regression of neovascularisation leaves ghost vessels or fibrous tissue. In most of the treated eyes, stable vision can be maintained once the retinopathy become quiescent, but the patients must be re-examined every 6–12 months [4]. Vitrectomy can prevent vision loss in patients with advanced stages of DR. Both laser photocoagulation and vitrectomy carry a risk of additional vision loss and also not effective in revising visual acuity loss [21]. Intraretinal steroid injections have shown temporary improvements in visual acuity in Diabetic Macular Edema (DME) patients. However, it may raise the intraocular pressure and develop cataracts [22]. Alternative treatment for DME is anti-Vascular Endothelial Growth Factors (anti-VEGF). There are many types of anti-VEGF are available. It inhibits the VEGF angiogenic activity by binding it to the VEGF protein and thus prevents its receptor activation [22,23]. Recent studies shows that anti-VEGF treatment can help to reduce DME and Age-related Macular Degeneration (AMD) [24].

1.4. Diabetic retinopathy screening systems

Manual diagnosis demands lot of effort to screen the images. Automated methods may reduce the time, cost and effort significantly [25]. The steady growth in diabetic cases has increased the growth of automated screening tools in recent years [25]. Moreover, Image processing, analysis, computer vision techniques and high end computing facilities are increasing in prominence in all fields of medical

science, and are especially relevant to modern ophthalmology to perform automated screening [26]. Philip et al. [19] proposed a systematic DR screening method. They studied the efficacy of the manual and automated “disease/no disease” grading system against the reference standard. Their automated system detected DR and maculopathy with an accuracy of 99.1% and 97.9% respectively. Abramoff et al. [27] developed a web-based screening tool for DR in a primary care population using Java programming language in Netherlands. The screening protocol contains a brief web-based questionnaire, visual acuity measurement, and four retinal images. These images were graded using browser and image processing tools and the results of the screening can be either not suspect and not urgent for normal class. In case of DR the result can be suspect and urgent. Their protocol obtained an interrater agreement (k) of 0.93. Abràmoff et al. [28] have proposed an evaluation method for automated DR detection using retinal fundus images in 10,000 diabetics. Their method obtained an Area Under Curve (AUC) of 0.84. The Early Treatment Diabetic Retinopathy study Protocol (ETDRS) was developed in United States to provide an efficient screening and validation procedures to analyze fundus images [9]. In Thailand, Suthanmmanas et al. [29] have developed an automatic DR tele-screening system in collaboration with National Electronic and Computer Technology Center [30]. This project used the internet technology to develop a reliable online screening system aimed to facilitate ophthalmologists of their country. Usher et al. [31] have developed DR screening tool with 1273 patients using the guidelines given by National Institute for Clinical Excellence, UK. Their method was able to detect DR with a sensitivity of 95.10% and specificity of 46.3%. Niemeijer et al. [32] have developed DR screening system using information fusion methods with 60,000 retinal images. Their software performed satisfactorily with an area under Receiver Operating Characteristic (ROC) of 0.881. Quellec et al. [33] have developed an automated instantaneous DR screening system using 2739 patients. This system was particularly used for detection of MA, drusen, and age-related macular degeneration and their software obtained an area under ROC of 0.927. Fleming et al. [34] have developed a Computer-Aided Diagnosis (CAD) system to detect blot HEM using 10,846 images obtained from Scottish DR screening centres: Glasgow, Tayside and Grampian. Their software was able to provide a sensitivity of 98.60% and a specificity of 95.50%. Fleming et al. [35] have developed a CAD system to detect MA using 1441 images obtained from Grampian diabetes retinal screening program. Images containing MA were detected with a sensitivity of 85.4% and specificity of 83.1%. Perumalsamy et al. [36] have developed Aravind Diabetic Retinopathy Screening 3.0 (ADRES3.0) CAD system using 210 images and achieved an accuracy of 81.3% by comparing the performance with ophthalmologists grading.

Several authors have reviewed different imaging methods, algorithms and their applications [37,38,26,39] for DR screening. Winder et al. [37] have reviewed various segmentation algorithms of Optic Disk (OD), retinal vasculature, macula, and detection of DR. Teng et al. [38] discussed retinal image preprocessing, segmentation of anatomical structures and abnormal lesions using fundus images, image registration, DR analysis and diagnosis algorithms. Abramoff et al. [39] reviewed different imaging modalities, detection of retinal vessels, abnormal lesions, performance of fundus image analysis methods, Optic Nerve Head (ONH) analysis, and Optical Coherence Tomography (OCT) image analysis. Patton et al. [26] reviewed retinal image preprocessing, registration, segmentation of land mark points and abnormal lesions, detection of pathology, measurement of retinal topography and its applications in telemedicine. However, in this review, we have discussed the recent methods to locate and segment the retinal image features namely OD, fovea, macula, blood vessels, hard and soft exudates, MA, and HEM comprehensively. Also, we have discussed DME detection, and automated detection of DR stages using retinal and OCT images respectively. We have also reviewed current treatment methods available for DME and DR. This paper has the following five sections: Section 2 briefly explains the retinal fundus imaging. The computational algorithms for detection and segmentation of basic anatomical structures and retinal lesions are explained in Section 3. Several image processing methods to detect and segment the OD, retinal vasculature, fovea, macula, hard and soft exudates, MA, HEM and detection of ME are also described in this section. Section 4 presents a detailed survey of the computer aided diagnosis of DR using above mentioned features and the review is finally summarized in Section 5.

2. Retinal imaging

Fundus imaging is a process where 3D structure of retina is projected onto the 2D plane. The image intensity represents the amount of reflected quantity of light [39]. The fundus camera consists of low power microscope and a camera is attached on the top of microscope. The optical design is similar to indirect ophthalmoscope, which provides vertical and magnified observation of inner surface of the eye. The camera views the retinal area at an angle of 30° to 50°, with 2.5 times magnification. It can be magnified up to 5 times using auxiliary lenses, using wide angle lens which can be viewed at from an angle of 15° to 140° [40]. The examining light is passed through a sequence of lenses followed by doughnut shaped aperture. Next the light is focused through a central aperture to create an annulus prior to objective lens of the camera and retina via cornea. The reflected light rays are focused through doughnut aperture of the illumination system. The image forming light rays travel in the direction of the low powered telescopic eyepiece [41,40]. The pupil is used to pass the illuminating and imaging light rays to the retina. The mirror present in the examining telescope redirects the light into film or charge coupled device to capture the image [41,40,39].

Color filters, fluorescein and indocyanine green dyes are used to perform the fundus imaging. The following modalities/techniques are used for retinal fundus photography for DR screening [39].

1. *Fundus photography (red-free)*—the image is captured using the amount of light reflected at a specific waveband [39].
2. *Color fundus photography*—the image is captured using the amount of reflected Red Green Blue (RGB) spectrum and the light sensitivity of the sensor [39].
3. *Fluorescein and indocyanine angiography*—the image formulated is based on the amount of emitted photons from fluorescein or indocyanine dyes, that are injected into the blood stream [39].

The correct adjustments of eyepiece and fundus camera focusing mechanism helps to get sharp fundus image. The eye and fundus camera must be focused on the reticle and film plane respectively, to produce a good quality image [41].

3. Detection and extraction of basic structures and clinical features

The screening system need to detect the anatomical structures such as fovea, OD and abnormal lesions such as MA, HEM, exudate, CWS, venous beading, fragile blood vessels and ME. Several authors have reported various segmentation methods to segment the anatomical regions and abnormal lesions. They are discussed briefly in the following sections.

3.1. Localization and segmentation of optic disk

Optic disk is used to diagnose serious eye disease such as glaucoma [42]. The shape of the OD may appear as circle or ellipse in the fundus image. The OD is also used as a reference point to locate the other anatomical structures such as fovea. It is located roughly 2.5 times of OD diameters from the temporal edge of the OD [43]. It can be used as a preceding information to determine the exact place of the macula, which is the central vision of the eye [43–45]. Moreover, OD localization helps to compute central retinal artery and vein equivalent [45,46]. The vessel tracking algorithms employ OD centre as reference point, because the retinal vessels are originated from the OD centre. The OD localization is performed by identifying the centre of OD or by drawing circle around the OD region. The OD segmentation is defined by determining the OD boundary using segmentation algorithms. Hence, detection and extraction of OD is significant [47,37].

3.1.1. Optic disk localization

The identification of OD is important to distinguish it from the other abnormal lesions. The OD localization methods described in the literatures are mainly identifying the approximated disk centre or the disk surrounded by a circle or square shape. In both cases, localization is difficult due to the presence of strong distractors such as vessel occlusions, imprecise boundaries, abnormal lesions like exudates and peripapillary atrophy [37,42]. The distractors normally have same characteristics of OD namely intensity, color and contrast. Previously, reported works in the literatures assume that the peripapillary atrophy region have high gray level variation than other region [48]. Usually OD is localized by grouping the bright pixels as a cluster. The algorithms based on intensity variations are simple, fast and reasonably robust for normal images with less intensity variations. These algorithms may fail when the OD is obscured by blood vessels and distractors like exudates, CWS and bright artefacts [49].

The OD color and shape can be used to identify OD from the distractors. Sinthanayothin et al. [50] have assumed 80 × 80 pixel as the size of OD and intensity variations of the neighboring pixels were used to localize the OD. The point with highest pixel variance was treated as OD centre and reported a sensitivity and specificity of 99.1%. Lowel et al. [45] have used correlation filter to locate the OD. Their method is able to identify OD in the fundus images which are affected with gross exudation, strong pallor and severe peripapillary atrophy. Hoover et al. [51] developed an algorithm using fuzzy convergence to identify OD after the application of illumination equalization. This algorithm detects the ONH using brightness characteristics of the ONH. Their proposed method achieved 89% correct detection. Walter et al. [52] developed an algorithm to identify OD using pixel brightness, discrete distance function and watershed transform in Hue,

Saturation, Luminance (HSL) color space. Their algorithm successfully localized the OD in all 30 images.

The Hough transform was used by many authors to detect OD (Lowell et al. [45], Charastek et al. [53], Ghafar et al. [54], and Treigys et al. [55]). The algorithm assumes many circles as edge points on the retinal image. These points are obtained using Sobel, Canny, Prewitt, Roberts and Log edge operators. Further, it decides the potential circle intersection with the OD and finally, the OD was located by effective voting of the edge points with highest vote [37].

Principal Component Analysis (PCA) was used for extracting different features present in the fundus images which includes OD and vessels (Sanchez et al. [56], Li and Chutatape [57], Sinthanayothin et al. [50]). PCA transforms the possibly correlated variable into uncorrelated variables called as principle components. The first principal component represents the maximum information present in the image. Li and Chutatape [57] extracted basic features present in the fundus image using PCA. The OD was correctly located with 99% accuracy.

Lalonde et al. [58] have proposed a pyramidal decomposition method with Hausdorff distance based template matching. Possible areas which might contain the OD were first found using pyramidal decomposition and Haar discrete wavelet transform with green band of the RGB image. They have reported the accurate identification of OD without OD boundary in all 40 images. The circular pattern was placed around the detected OD region. Lowell et al. [45] have showed similar results with less complex methods than pyramidal decomposition and template-matching.

Foracchia et al. [59] have described an algorithm by modelling geometrical directional pattern of the main vessels. Initially, the vascular skeleton was extracted to measure the diameter, centre point and direction of the vessel. The main blood vessels modelled using parabolas were used to identify the centre of the disk [37,59]. They reported an accuracy of 98% in localizing the OD (79 out of 81 images) and located OD position using the prior knowledge obtained from the anatomical structure.

Youssif et al. [60] have proposed an algorithm using vessel direction. The disk was detected correctly with an accuracy of

98.77% using STructured Analysis of the Retina (STARE) dataset and 100% using Digital Retinal Images for Vessel Extraction (DRIVE) dataset by matching the vessel pattern at OD vicinity.

Fleming et al. [61] have proposed an automated OD localization algorithm using temporal arcade detection and semi-ellipse fitting. The vessel enhancement was performed in green channel images. The intensity gradient of the vessel wall, vessel width were used to locate the temporal arcade. Further, semi-elliptical shape of the arcades was identified using Hough transform. The local gradient information and direction of the vessels were combined with circular Hough transform to localize the OD.

The parts of the fundus photographs such as OD, the macula, and the vascular arch were automatically located by [62]. Their algorithm detected the OD with an accuracy of 98.4% and 94% for normal and DR images respectively [62].

3.1.2. Optic disk segmentation

Optic disk boundary extraction is commonly carried out by subsequent localization of the OD. Identifying the boundary of the OD is an important problem.

OD segmentation using active contours or snake have been experimented by many authors (Lowell et al. [45], Mendels et al. [63,64], Joshi et al. [42]). Primarily, Kass et al. [65] developed an active contour model or snakes that expand or shrink based on image and contour properties. The internal and external energy function controls the behavior of the parametric active contours. The active contour model is susceptible to the initialization and also limiting the search space, which results in enhanced final contour. Further, Xu and Prince [66] have proposed Gradient Vector Flow (GVF) whose curves can be initiated by the contour points. It converges or expands based on internal and external forces present in the image. GVF is one of the external forces for traditional snake that has ability to progress into boundary concavities by taking into consideration the direction as well as magnitude of gradients [66]. The snake initialized around the OD and GVF can be used to fit the contour with the rim of the disk [63,64].

A modified Active Shape Model (ASM) was developed [57] to locate the OD boundary in fundus images. ASM involves building

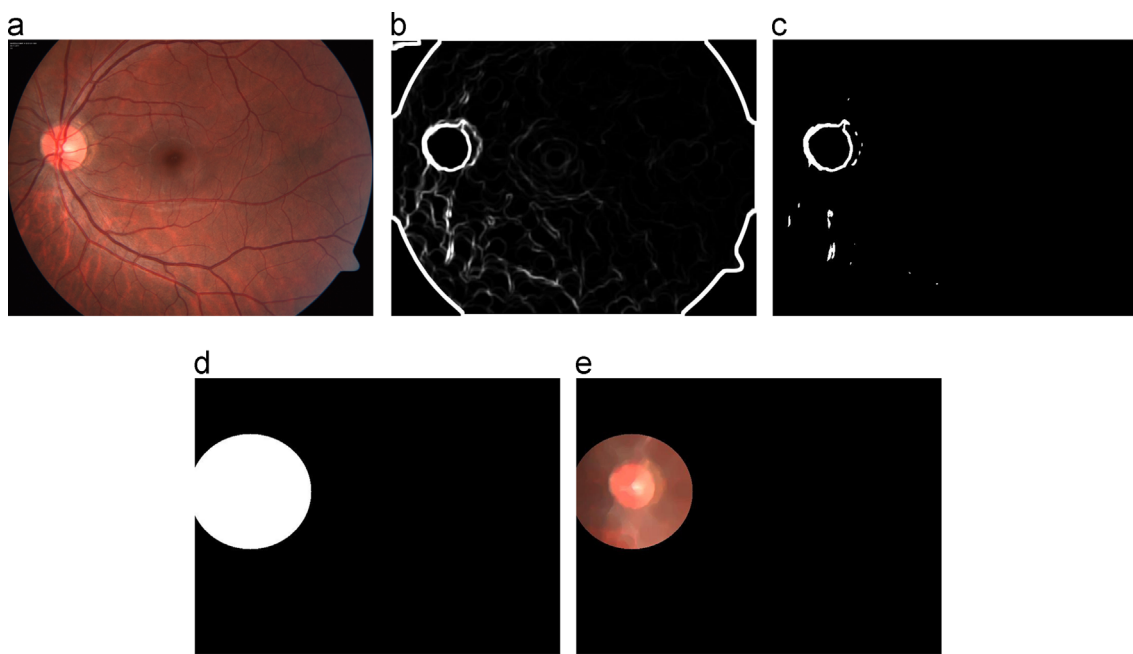


Fig. 2. (a) Normal; (b) CWNO processing result; (c) Thresholding result; (d) OD mask; (e) Isolated OD.

of Point Distribution Model (PDM) using sample data and recurrent searching to locate occurrence of disk like shapes in the fundus image. Further, PCA was performed to represent the total variance of the training shapes. This algorithm yielded an accuracy of 94% [57].

Attanassov Intuitionistic Fuzzy Histon (A-IFSH) method [67,68] was used to segment OD. The contour of OD was segmented using two-step approach. During preprocessing stage Contrast Limited Adaptive Histogram Equalization (CLAHE) was performed on the original image (Fig. 2a) [69] and blood vessels were removed using morphological closing followed by segmentation using 2D matched filter [70]. The Column Wise Neighborhood Operation (CWNO) was applied to remove background leaving only the border and OD (Fig. 2b). Thresholding ($T=0.5$) was carried out (Fig. 2c) to get the OD edge. The circular mask with 150 pixel radius (Fig. 2d) was generated using the OD edge information. This mask was subtracted from image (Fig. 2a) to isolate the OD region (Fig. 2e).

Further, pixel hesitancy was modelled by A-IFSH method. To segment the OD, roughness index (Fig. 3a–c) was computed by correlating the histogram and A-IFSH. The region between two valley points represents the OD region. Using this information OD was segmented (Fig. 3d, e) and their algorithm detected the OD in all 100 images correctly. Fig. 2a shows the original image; Fig. 3d indicates segmented OD using A-IFSH algorithm and Fig. 3e depicts the segmented OD subtracted from Fig. 2a. Their algorithm yielded an accuracy of 93.4% and its performance was compared with Otsu and GVF snake methods.

Lee et al. [71] have proposed an OD segmentation method in two stages. Initially, the blood vessels were removed which obscure the OD. Next, the edge points of the disk boundary were detected to extract the disk. Their algorithm extracted the disk with an accuracy of 92% [71].

Walter and Klein [52] have described the disk segmentation using watershed transform. They have segmented the contour of the OD with minor distortion due to obscured vessels and low contrast in 27 out of 30 images. The OD localization and segmentation methods are summarized in Table 2.

3.2. Segmentation of retinal vasculature

The accurate segmentation and measurement of blood vessels is important to diagnose systemic and ophthalmologic conditions. Length, diameter, path, changes in vessels during progression of DR are significant diagnostic indices of the disease. The vessel segmentation methods can be divided in to five groups: vessel tracking, mathematical morphology, matched filtering, model-based thresholding or deformable models, and supervised pixel classification methods. They are briefly discussed below.

Vessel tracking methods: (Tolias et al. [72], Englmeier et al. [73], Vlachos and Dermatas [74], and Nayebifar et al. [75]) tried to obtain the vascular structure by identifying vessel centre lines. The blood vessel searching was initiated by set of seed points. Vessels were traced by local information of the pixels that are close to the one currently under assessment. Vessel tracking methods rely on the seed point selection, which decides the vessel segmentation accuracy.

Mathematical morphology: Zana and Klein [76] used mathematical morphology to segment blood vessels. The known vasculature shape features namely piecewise and connections were used to select the structuring element for morphological filtering. Their algorithm is a combination of mathematical morphology and cross-curvature evaluation to segment blood vessels in retinal images. The morphological filters simplify the image so that the cross-curvature computation is easy and also the vessel segments are linearly coherent. In this method selection of proper structuring element is important to obtain better segmentation.

Matched filtering: The 2D-matched filter was used by several authors to detect retinal vasculature (Chaudhuri et al. [70], Al-Rawi and Karajeh [77], Osareh and Shadgar [78], Hoover et al. [79], Mookiah et al. [80], Gangand et al. [81], Zhang et al. [82], and Zhang et al. [83]). The gray level profile of the blood vessel was modelled using Gaussian and two dimensional Gabor filters, which provides 12 templates to extract vessels [70] from the fundus image. Li et al. [84] used a piecewise Gaussian model for blood vessel segmentation and Mahalanobis distance classifier for final segmentation. Gangand et al. [81] measured the vessel diameter using matched filter, which showed

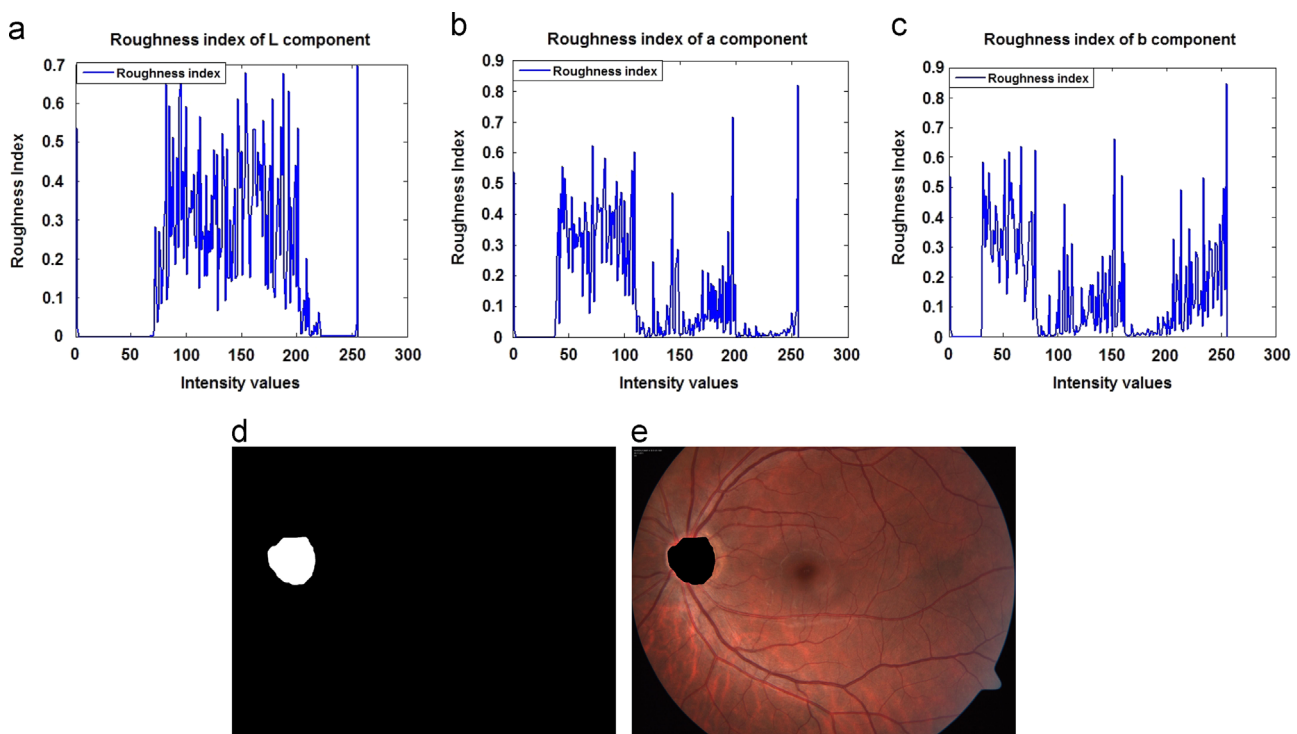
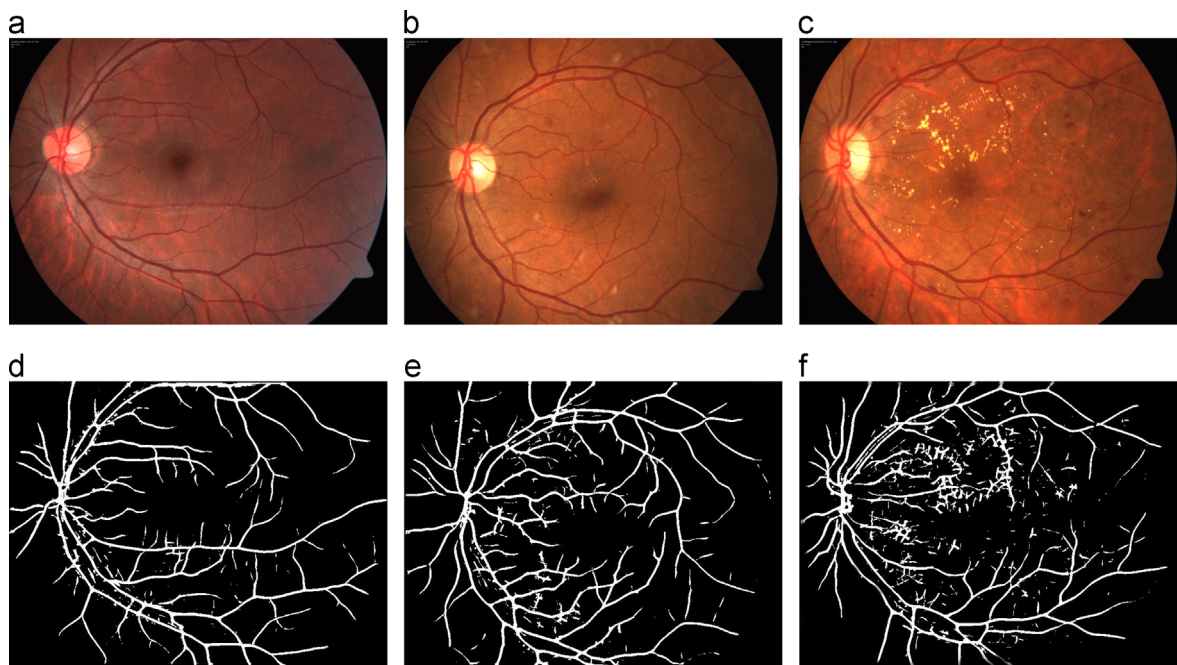


Fig. 3. (a), (b) and (c) Roughness index plotted against intensity; (d) Extracted OD; (e) OD subtracted from (Fig. 2a).

Table 2

Performance measures of OD localization and segmentation methods.

Authors	Methods (dataset size)	Salient feature	Performance measure
Optic disk localization			
Sinthanayothin et al. [50]	Highest average variation (112)	The adjacent pixels variance used for localization	Sensitivity-99.1%
Walter and Klein [52]	Pixel brightness and discrete distance function (30)	Area threshold	Specificity-99.1%
Lalonde et al. [58]	Pyramidal decomposition with Hausdorff-based template matching (40)	Dempster-Shafer theory	Accuracy-100%
Hoover et al. [51]	Fuzzy convergence (81)	Identifies vessel without strong convergence	Accuracy-89%
Foracchia et al. [59]	Modelling the direction of main vessels (81)	New model to identify vessel direction	Accuracy-98%
Li and Chutatape [57]	PCA (89)	PCA to detect the OD	Accuracy-99%
Fleming et al. [61]	Image gradient and Hough transform (1056)	Temporal arcade direction	Accuracy-98.4%
Niemeijer et al. [62]	2D Single point-distribution-model (500)	Cost function and minimization strategy	Accuracy-98.4%
Treigys et al. [55]	Canny edge detector and Hough transform (54)	Non-static thresholding	Accuracy-98%
Youssif et al. [60]	2D Gaussian matched filter and morphological operations (81)	Directional model of vessels	Accuracy-98.77%
Optic disk segmentation			
Mendels [63]	Morphological operations and active contours (9)	Hierarchical adaptive mesh structure generation	Accuracy-100%
Walter and Klein [52]	Watershed transform (30)	Area threshold	Accuracy-90%
Li and Chutatape [57]	Modified active shape model (89)	Detects weak edges	Accuracy-94%
Lowel et al. [45]	Deformable model based segmentation algorithm (90)	Use of energy function and Quasi-Newton optimization strategy	Accuracy-83%
Charastek et al. [53]	Active contour model and Hough transform (159)	Can judge the image quality and distinguish the image with large and small ONH	Accuracy-72.3%
Lee et al. [71]	Morphological operations and spline interpolation (23)	Can detect oval, ellipse and circle OD contours	Accuracy-92%
Joshi et al. [42]	C-V model (138)	Model works without imposing any shape constraint	F-score-0.97
Mookiah et al. [67,68]	A-IFSH (100)	Uses fuzzy image representation	Accuracy-93.4%

**Fig. 4.** (a) Normal; (b) Moderate NPDR; (c) Severe NPDR; (d) Segmented blood vessels from (a); (e) Segmented blood vessels from (b); (f) Segmented blood vessels from (c).

that the inclusion of the width measurement improved its performance and resulted in better detection. Zhang et al. [83] used truncated Gaussian function to modify the matched filter. The background subtraction was achieved by matched filter response and thresholding. This method initially uses Gaussian filter and double sided thresholding to improve image quality and extract different features present in the image. It significantly reduced the false detection. Al-Rawi et al. [77] have improved matched filter response by tuning the filter parameters using Genetic Algorithm (GA). The

matched filtering was used to segment [80] normal, NPDR and PDR images and its results are shown in Fig. 4d, e, f respectively.

Wu et al. [85] have proposed adaptive blood vessel detection method for large and small blood vessels. Initially, the vessels were enhanced using adaptive histogram equalization. Further, the vessels were modelled using standard deviation of Gabor filter response at different orientations. Finally, three major operations such as forward detection, backward verification and bifurcation detection were performed to segment out the vessels.

This method has following advantages and limitations: (i) specular bright reflex of the vessels can be eliminated by this method; (ii) at least 4–6 templates are needed to have a reasonably good enhancement of vessel segments; (iii) selection of proper thresholding scheme to distinguish enhanced linear segments of vessel and remaining part of the image; (iv) detected blood vessels have good edge localization; (v) applicable only to stationary processes.

Niemeijer et al. [86] have compared five different blood vessel detection methods such as matched filter, Scale-space analysis and region growing, mathematical morphology and curvature estimation, verification based local thresholding and pixel classification using DRIVE database. They reported that pixel classification method performed better than other methods.

Model-based thresholding and deformable models: Multi-concavity modelling method [87] was used to detect blood vessels. The line-shape concavity measure was proposed to remove dark lesions and locally normalized concavity measure was used to remove noise. These concavity measures were combined together to detect vessels in retinal images. Goatman et al. [88] have proposed a methodology to detect abnormal vessels in the OD region. The empirically derived threshold was applied for segmentation of the vessels, which produced many disjoint vessels. To overcome this problem, watershed transform was applied [52,89]. To avoid over segmentation, two dimensional Gaussian filter was applied on inverted image. Martinez-Perez et al. [90] proposed a method using derivative features of the image and two-stage region growing to extract vessels from red-free and fluorescein photographs. The active contour model or snake [91,92] was used to detect blood vessels. The tram-line algorithm [91] extracted a pixel map consisting of sparse lines roughly along vessel centres. This map was further processed to produce a vascular segment map, each section identifying a precise centreline of vessel segment and diameter along the length of the vessel. Ribbon of Twins method [92] was initialized using morphological filters to identify the centre line of the vessels. Once the vessel segments were identified, the network topology was determined using an implicit neural cost function to resolve junction configurations. The vessel detection accuracy of the model-based algorithms mainly depends on the selection of the best model parameter.

Supervised pixel classification: The supervised ridge-based vessel detection [93] assumes that the vessels are elongated structures. Initially, the ridges were extracted and the ridge pixels were grouped into patches. Features were computed from each pixel and sequential forward selection was used to identify the best features. Feature vectors (pixels) were classified using k -Nearest Neighbor algorithm (k -NN) into vessel or non-vessel pixels. Soares et al. [94] developed a vessel detection method using 2-D Gabor wavelet and Gaussian Mixture Model (GMM). The Gabor wavelet can be tuned to specific frequency to filter noise and enhance vessel in single step. The gray values and filter response at different angles and scales were used as features. Marin et al. [95] proposed an algorithm to detect vessels using gray values and moment invariant features. The Neural Network (NN) was used to detect vessel and non-vessel pixels using the extracted features. Ricci and Pefetti [96] have used Support Vector Machine (SVM) to classify vessel or non-vessel pixels. The features were extracted using two orthogonal line detectors. Finally, Rossant et al. [97] have proposed unsupervised vessel extraction algorithm using filtering and path-opening. The noise and small walls which may affect the vessel segmentation were suppressed by Gaussian filter. Before applying path-opening filter, morphological operations and adaptive filtering were used to enhance the vessels in the inverted image. The path opening filter was applied to retain the elongated bright structures whose length was larger than 40 pixels. Finally, classification and fusion are applied to reconstruct the segmented blood vessels. The pixel classification performance can be maximized by tuning the classifier parameters. The summary of the retinal vascular segmentation methods is presented in Table 3.

3.3. Localization of the macula and fovea

The macula may appear as oval-shaped yellow pigmented region near centre of the retina around the fovea (Fig. 1a). It is small and responsible for central and high resolution vision. The visual cells located in the fovea are packed tightly, resulting in optimal sharpness of vision [98]. The macula does not have blood vessels to interfere the passage of light striking the foveal cone mosaic [99]. The macula localization methods can be divided in to two groups: hybrid approach-based and positional constraints-based methods. The macula is a dark and circular region with low contrast and distracted slightly by exudates or HEM. The fovea is placed around 2–2.5 times of OD diameter to the temporal edge of OD [50,57,62,100–102].

Hybrid approach-based: Sinthanayothin et al. [50] have proposed an algorithm to locate fovea using intensity correlation. Initially, fovea is subjected to intensity correlation and the peak was selected from Hue Saturation Intensity (HSI) transformation. This peak point location is a dark region and considered as fovea [50]. Their algorithm failed when the fovea is not centred. A polar fundus coordinate system was developed using foveal location [57]. The fovea is localized accurately using its appearance (dark) and its geometrical relation to other structures [57]. Niemeijer et al. [62] have developed an algorithm to locate macula using single point distribution model. Their model consists of global and local cues, to locate the model points. These cues were derived from the relative physical position and width of the vessel model and structure. This method was able to localize macula in both eyes with OD and macula centred images.

Positional constraints-based: The positional constraints [50,57, 62,100–102,61] were used to identify the macula and determines the position, and variation in the OD size. The macula and fovea detection was achieved using the physical position of other parts of the image. The primary approach of this algorithm [103] determines the horizontal retinal ridge passing through the optic nerve and fovea, which separates the upper and lower retinal parts. Further, the foveal region was estimated using fixed distance of 2.5 OD diameters from the central optic nerve coordinate [50,57,62,100–102,61]. To determine the retinal raphe, authors have applied a parabolic model. This method is robust to wide variety of pathologies. The summary of the macula and fovea detection methods is presented in Table 4.

3.4. Segmentation of hard and soft exudates

This section summarizes literatures of exudates segmentation. Exudates are prime markers of DR, since it causes retinal edema and subsequently loss of vision. Exudates segmentation methods can be divided in to three groups: clustering-based, mathematical morphology and thresholding/region growing-based, and pixel classification-based methods. They are briefly explained below.

Clustering-based: Several authors [104–106] have used FCM clustering for exudates segmentation. This algorithm considers pixels with diverse classes and varying degrees of membership for segmentation [107,108]. Osareh et al. [104] have corrected color and contrast during preprocessing. The preprocessed color images were segmented using FCM and the clustered regions were classified to exudates and non-exudates regions using NN. The GA was used to select best features from FCM clustered regions [105]. Further, the optimum features were fed to the NN to identify exudates and non-exudates regions. This method tackles the varying retinal color, which may be due to skin pigmentation or iris color. The exudates were detected from poor quality images, which were taken from eyes without dilation using FCM [106]. Initially, preprocessing was performed to improve the contrast and four intensity based features extracted for clustering. The same group reported exudates segmentation using naive Bayes classifier [109]. Hsu et al. [25] have developed an automated exudate

Table 3

Performance measures of retinal vasculature segmentation methods.

Authors	Methods (dataset size)	Salient feature	Performance measure
Segmentation of retinal vasculature			
Tolias et al. [72]	Fuzzy C-Means (FCM) (3)	No initialization and vessel profile modeling problems	Detection ratio-79.41%
Hoover et al. [79]	Matched filter and piecewise thresholding (5)	Uses local and region-based properties	Sensitivity-80%, specificity-90%
Gangand et al. [81]	Amplitude-modified second-order Gaussian filter (48)	Vessel width measurement is used	Accuracy-85.50%
Hunter et al. [91]	Tram-line algorithm (20)	Robust against edge distractors	Accuracy-57.20%
Li et al. [84]	Piecewise Gaussian model and Mahalanobis distance classifier (505)	Central reflex characteristics	Success rate for arteries-82.46% veins-89.03%
Englmeier et al. [73]	Blood vessel pixel brightness (213)	Performs well with discontinuous edge and noisy regions	Accuracy-78.40%(Artery) Accuracy-66.50%(Veins)
Staal et al. [93]	Ridge detection and k-NN classifier (40)	Robust with primitive based method and leave-one-out feature selection	Area under ROC-0.952
Soares et al. [94]	Gabor wavelet transform and Bayesian classifier (60)	Gabor wavelet segments vessel with different diameters	Area under ROC-0.9614
Wu et al. [85]	Gabor filter response (20)	Small and large vessel can be detected	True Positive Rate (TPR)-84.3% False Positive Rate (FPR)-3.9%
Al-Rawi and Karajeh [77]	Two-dimensional matched filter and genetic algorithm (40)	Able to tune matched filter parameters of other medical images	Accuracy-94.22%
Martinez-Perez et al. [90]	Multi-scale feature extraction, Geometric properties of blood vessels and multipass region growing (114)	Detect vessels with different widths	TPR-75.05%(STARE), FPR-4.38%(STARE), TPR-72.46%(DRIVE), FPR-3.45%(DRIVE)
Ricci and Perfetti [96]	Line operators and SVM (60)	Robust to noise and other artefacts	Accuracy using DRIVE-95.95%, accuracy using STARE-96.46%
Al-Diri et al. [92]	Ribbon of Twins active contour model (40)	Accurately locate vessel edges and closely parallel fine vessels	Sensitivity using DRIVE-72.82%, sensitivity using STARE-75.21%
Osareh and Shadgar [78]	Gabor filters and SVM (90)	Suitable when the system needs to be adapted for new datasets	Sensitivity-96.50%, specificity-97.10%
Lam et al. [87]	Multi-concavity modelling (60)	Can identify vessels with bright and dark retinal lesions	Accuracy using DRIVE-94.72%, accuracy using STARE-95.67%
Vlachos and Dermatas [74]	Multi-scale line-tracking (40)	Robust with salt/pepper noise and low signal to noise ratio	Sensitivity-74.70%, specificity-95.50%, accuracy-92.90%
Goatman et al. [88]	Thresholding and watershed transform (109)	Can detect new vessels at the OD	Sensitivity-84.20%, specificity-85.90%
Marin et al. [95]	Gray level and moment invariant based features and NN (60)	Invariant to scale and work with different resolution images	Accuracy using DRIVE-94.52%, accuracy using STARE-95.26%
Rossant et al. [97]	Top-hat transform and path-opening morphological filter (40)	Unsupervised blood vessel segmentation	Sensitivity-70.31%, specificity-97.88%, accuracy-94.33%

Table 4

Performance measures of macula detection methods.

Authors	Methods (dataset size)	Salient feature	Performance measure
Localization of the macula and fovea			
Sinthanayothin et al. [50]	Intensity correlation (112)	Correlation coefficient is independent of image contrast	Sensitivity-80.40%, specificity-99.10%
Li and Chutatape [57]	Pixel intensity and geometrical relation (89)	Better fovea detection due to fundus coordinate system	Accuracy-100%
Fleming et al. [61]	2D Gaussian and region growing (1056)	Main vessel arcade was used to find the fovea	Accuracy-96.5%
Niemeijer et al. [62]	2D Single point-distribution-model (500)	Better macula detection due to cost function and minimization strategy	Accuracy-94.40%
Tobin et al. [103]	Positional constraints and parabolic model (345)	Performs well with erroneous optic nerve coordinate detection	Accuracy-92.50%

segmentation method using clustering and domain knowledge. Initially, median filtering was used to compute the intensity difference map. Next, dynamic clustering was applied to group the lesion pixels. The contrast information of the lesions such as hard exudates, CWS and drusen were used to differentiate the lesion. Hard exudates have higher intensity than other two lesions, this information was used to segment out exudates. The limitation of these techniques is to identify significant clusters which contribute to the segmentation of exudates.

Mathematical morphology and thresholding/region growing-based: Mathematical morphology [110–112] and thresholding/region growing techniques [113,80] were used by many authors to segment exudates. Sopharak et al. [110] proposed an exudates detection method for poor quality images obtained from eyes

without pupil dilation using optimally adjusted morphological operators. Walter et al. [111] identified exudates using gray level variations of green band images. After initial identification, their boundaries were identified using morphological reconstruction methods. Their algorithm did not discriminate exudates from CWS. Sanchez et al. [112] have applied Walter et al. [111] segmentation method. Initially, the green band image was pre-processed and the histogram of the processed image was modelled using GMM. Further, variable threshold was used to extract the exudates using the knowledge obtained from GMM. Sinthanayothin et al. [113] applied a Recursive Region-Growing Technique (RRGT) on a 10×10 window using selected threshold values in gray scale images. Adaptive local contrast enhancement was

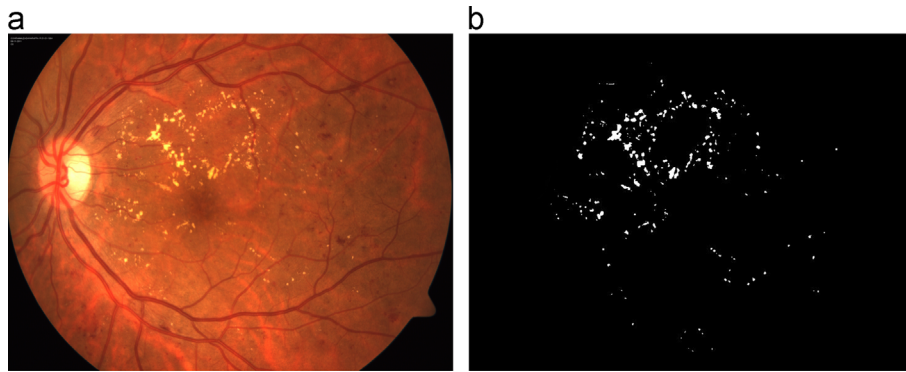


Fig. 5. (a) Severe NPDR; (b) Segmented exudates from (a).

used to enhance the image quality. This method localizes other anatomical regions such as OD, blood vessels and fovea.

Fleming et al. [114] have proposed a multi-scale morphology method to locate exudates in retinal fundus images. Their method uses median and Gaussian filtering of green channel image to correct the shading and contrast variations. Further, multiple linear structuring element opened with a single disk shaped structuring element was used to detect the exudates. Then, watershed retinal region growing was applied to isolate the exudates from vessels and other regions. Finally, the detected regions were classified into exudates, drusen and background using SVM classifier.

Welfer et al. [115] have proposed an automated exudate detection method based on mathematical morphology. First the images were subjected to contrast enhancement in Luv color space. Then a set of morphological operations such as regional minima detection, morphological reconstruction and H-maxima transform were performed to detect exudates. Their method was evaluated using DIAbetic RETinopathy DataBase Calibration level 1 (DIARETDB1) database.

Mookiah et al. [80] have proposed exudates segmentation using color, shape and morphological processing. The algorithm assumes exudates to have higher contrast than OD. The OD was segmented and removed using A-IFSH algorithm [68]. First, circumferential retinal region was removed by mathematical morphology and fixed threshold of 0.35 was used to extract exudate (Fig. 5b). However, the performance of the above mentioned methods mainly relies on selection of proper structuring element and threshold value which separates the exudates and background regions.

Pixel classification-based: Several authors [116–118] have used machine learning methods to classify exudates and non-exudates pixels. Gardner et al. [116] have used NN to segment exudates. The exudates were identified using gray scale values of fundus images. The mask of 20×20 region was used to isolate exudates. Sanchez et al. [118] have identified exudates in color retinal images based on Fisher's Linear Discriminant Analysis (FLDA). Before doing this, authors have performed color normalization and contrast enhancement in modified RGB model. Hard exudates were mainly recognized by its color. Hence, the feature space was defined using color. The selection of color model is a complex task and hence authors have used quantitative metric to identify the best color space. It involves extensive computation during training and classification. Moreover, the performance can be maximized by tuning the classifier parameters.

Niemeijer et al. [119] have proposed an automated detection and differentiation of exudates, CWS and drusen using pixel classification based on machine learning algorithm. Initially, pixels were classified and lesion probability map was generated which shows that the pixels belongs to bright lesions. Next, high probability pixels were grouped into probable lesion pixel clusters. Finally, the likelihood of the pixel clusters were computed to

discriminate exudates, CWS and drusen. The summary of the hard and soft exudates segmentation methods is presented in Table 5.

3.5. Segmentation of microaneurysms and hemorrhages

Earlier, automated retinal lesion detection was conducted using fluorescein and red-free photographs [120]. Preliminary global image processing methods were applied for automated detection. Many researchers have investigated the extraction of MA and HEM from the fundus images by thresholding after removing the parts of the retina namely OD, fovea, macula, and blood vessel. Mathematical morphology was applied to the thresholded image to discriminate MA and other features, like small vessel sections. The MA segmentation methods can be divided in to four groups: mathematical morphology-based, region growing-based, wavelet-based, and hybrid approach-based methods. The HEM segmentation is mainly based on mathematical morphology and pixel classification. They are briefly explained below.

Mathematical morphology-based: Walter et al. [121] have proposed four step algorithm for the detection of MA. In preprocessing stage polynomial contrast enhancement was applied on green channel image. The top-hat transformation was applied on the diameter closed image to locate MA. Global thresholding was applied to segment MA, fifteen shape and color features were used to distinguish real MA from other lesions using k-NN, Gaussian and kernel density estimation based classifiers. This algorithm was able to discriminate possible MA from vessel-like patterns. Hatanaka et al. [122] have developed an automated HEM detection method using brightness correction. Initially, the brightness was adjusted in HSV space. Further, the fundus image was smoothed using 3×3 mask. Further, the blood vessels and HEM were segmented using thresholding.

Region growing-based: Fleming et al. [35] have described contrast normalization, watershed and region growing methods to segment out MA in retinal photography. The images were convolved with 2D Gaussian after median filtering. The contrast was normalized using its standard deviation. Region growing was performed on the watershed gradient image to grow the candidate regions. The k-NN classifier was used to detect MA using nine extracted features from candidate regions. Adapting this method to HEM segmentation requires the estimation of other lesion boundaries. Sinthanayothin et al. [113] have used RRGT and adaptive intensity thresholding combined with a moat operator to detect MA. The moat operator enhances the edges obtained by the contrast of the lesions.

Wavelet-based: Quellec et al. [123] have described a MA segmentation algorithm in retinal photographs using optimal wavelet transform. The sub-bands of wavelet transformed images were locally matched

Table 5

Performance measures of exudates segmentation methods.

Authors	Methods (dataset size)	Salient feature	Performance measure
Segmentation of hard and soft exudates			
Gardner [116]	NN (301)	Statistical threshold tuning	Sensitivity-93.10%
Hsu et al. [25]	Clustering and contrast information (543)	Domain knowledge	Sensitivity-100%, specificity-74%
Sinthanayothin [113]	RRGT and moat operator (30)	Use of moat operator	Sensitivity-88.50%, specificity-99.70%
Walter et al. [111]	Pixel variations (30)	Accuracy depends on minimal variation value and contrast	Sensitivity-92.80%, predictive value-92.40%
Osareh et al. [104]	FCM (142)	Locate exudates at pixel resolution	Sensitivity-93%, specificity-94.10%
Sanchez et al. [56]	Color and statistical classification (80)	Threshold selection based mixture model	Sensitivity-79.62%
Fleming et al. [114]	SVM (13219)	Drusen also can be detected	Sensitivity-95%, specificity-84.6%
Sanchez [118]	Color and FLDA (58)	User initialization is not required and robust	Sensitivity-100%, specificity-100%, accuracy-100%
Niemeijer et al. [119]	Pixel classification (300)	Detects and differentiates exudates, CWS and drusen	Exudate detection: sensitivity-95%, specificity-86%, CWS detection: sensitivity-70%, specificity-93%, Drusen detection: sensitivity-77%, specificity-88%
Sopharak [110]	Optimally adjusted morphological operators (60)	Works well even with poor computing system	Sensitivity-80%, specificity-99.50%
Sopharak [109]	Naive Bayes classifier (39)	Works well even with non-dilated fundus images	Sensitivity-93.38%, specificity-98.14%, accuracy-98.05%
Osareh et al. [105]	FCM, shape, NN (300)	Distinguish CWS and exudates using edge strength and texture	Sensitivity-93.50%, specificity-92.10%
Sanchez et al. [112]	Histogram modelling and dynamic thresholding (20)	Uses minimum distance discriminant criteria	Sensitivity-100%, specificity-90%
Sopharak [106]	FCM (40)	Quantifies pixel similarity using distance between pixels and cluster centre	Sensitivity-92.18%, specificity-91.52%
Welfer et al. [115]	Mathematical morphology (88)	Course and fine exudate detection	Sensitivity-70.48%, specificity-98.84%

with the lesion template to detect MA. This algorithm detects MA without extracting and classifying the candidates. Hansgen et al. [124] have studied the use of wavelet in fundus image compression and its effects on the automated MA segmentation. They have employed (i) Discrete Wavelet Transform (DWT) (ii) Industry standard Joint Photographic Experts Group (JPEG) techniques. Further, the uncompresssed images were experimented to segment MA. JPEG compression was used to detect the MA [124] with higher accuracy.

Hybrid approach-based: Spencer et al. [125] have developed an algorithm based on mathematical morphology and matched filter to segment MA using fluorescein angiograms. Initially, the morphological operations such as erosion followed by dilation was performed on shade-corrected image. An 11×11 Gaussian shape was correlated with an image after top-hat transformation. Further, matched-filtering was applied followed by region growing to segment out MA. Frame et al. [120] applied Spencer et al. [125] method to detect MA after correcting illumination variations. The classification methods viz., Linear Discriminant Analysis (LDA), NN and Rule based analysis were used to classify the objects like MA. Using their method it is difficult to distinguish small MA with background fluorescence patches. Cree et al. [126,127] have refined the technique proposed by Spencer et al. [125] using alternative region growing and classification algorithms in fluorescenin images by adding four intensity-based measurements, which were scaled by contrast of the image. Their technique was able to discriminate MA from micro-vascular abnormalities. Niemeijer et al. [117] have presented a hybrid red lesion segmentation algorithm using Spencer et al. [125] and Frame et al. [120] methods. Initially, the red lesion candidates were detected using pixel classification [125]. After applying this method, vessels and red lesions were isolated from the background. Further, the red lesions were extracted after discarding the connected vasculature. In addition to the features of earlier methods [125,120] additional features were used to identify red lesions using k-NN classifier. Usher et al. [31] used NN to detect MA. Initially, preprocessing

performed by locally adaptive contrast enhancement and segmentation of OD and vessels, HEM/MA were performed using RRGT and adaptive intensity thresholding combined with moat operator [113]. Features such as size, shape, hue and intensity were derived to detect MA using Artificial Neural Network (ANN). The specific detection of sight-threatening maculopathy was also achieved using this algorithm. Zhang et al. [128] have proposed an approach using Multi-Scale Correlation Filtering (MSCF) and variable threshold within fluorescein angiography. In the course level, the authors detected MA using MSCF. The correlation coefficient of the pixels were extracted using sliding window Gaussian kernels with different scales. In the fine level, 31 features were extracted from the detected MA, to manually classify true and false MA using fixed threshold value. This algorithm worked independent of image condition and resolution. Hence tuning of parameters are not needed to achieve the improvement. Streeter and Cree [129] have proposed a MA detection approach using shading correction, top-hat transform, matched filter and region growing to enhance small round features after background intensity correction. Further, LDA was used to detect true MA which can classify only MA of greater than ten pixels in size. Lazar and Hajdu [130] have proposed an automated MA detection method using directional cross-section profile centred on the local maximum of the image pixels. Peak detection was applied on the profiles to compute size, shape, and height features. Finally statistically significant features were fed to naive Bayes classifier to identify the MA. The proposed method was able to distinguish blood vessel bifurcation and crossings from MA. Larsen et al. [131] have proposed an automated MA and HEM detection method using RetinalLyze System. The shape and size of the lesions were used for classification. Their system was unable to distinguish the two lesions.

Mathematical morphology-based and pixel classification-based: Fleming et al. [34] have used multiscale and morphological techniques to detect HEM During preprocessing the changes in image intensity and contrast was corrected using median filtering and histogram

equalization. Further, morphological operations were performed to extract HEM. The algorithm proposed in [35] was used to detect large abnormal regions in different scales by iteratively applying various structuring elements. Two stages of region growing were performed [35] to detect the lesions. Using this approach distinguishing HEM from smaller dark lesions was difficult. Zhang and Chutatape [132] have developed an algorithm to segment out HEM using SVM. During preprocessing color normalization was performed to find pixel evidence value. Further, two dimensional PCA was used to extract the features. These features were fed to SVM to segment out HEM. Rotation and illuminance invariance were employed to get virtual support vectors, which improved the classification accuracy. Hipwell et al. [133] have developed an automated MA technique in digital red-free fundus images. Initially, the images were subjected to shading correction to remove changes in the illumination. Next, vessels and HEM were removed by excluding all structures greater than MA. Finally, the objects having size and shape of MA were retained for classification. Antal and Hajdu [134] have developed an ensemble based MA detection algorithm. The ensemble creation was performed by preprocessing and candidate extraction. Euclidean distance was computed between the pairs for the ensemble having more pairs. The candidates were grouped together, if their distance is less than that of predefined constant. These ensembles were compared with the ground truth to detect MA. Gardner et al. [116] used NN to segment MA and/or HEM.

The results of first international MA detection competition were discussed in [135]. The results of five different methods such as Valladolid [136], Waikato [137], Latim [123], Ok Medical [138], and Fujita Lab [139] presented by five different teams of researchers were discussed. They used same dataset to evaluate their algorithms, 50 training and 50 test images. Valladolid [136] used green channel image and normalized the image by subtracting an median filter estimate from the background. The MA detection was performed using GMM and thresholding. Waikato [137] MA detector used green plane images for MA segmentation. Initially, the noise was removed using median filtering. Further, top-hat transform was used to identify the vessels and subsequently it was removed. Finally, matched filtering was used to detect the MA and region growing was used to segment the MA. Latim [123] MA detector assumes that MA is at a particular scale and can be modelled using 2D Gaussian functions. Further, it uses template matching in the wavelet domain to identify the MA candidates. Ok Medical [138] MA detection method uses a multiscale Bayesian correlation filtering. The probabilistic model of MA and its surroundings were modelled using Gaussian filterbank. Further, correlation measure was obtained by matching the filterbank output with the new image. Finally, the MA was segmented by thresholding correlation filter output. Fujita Lab [139] method starts with brightness correction, gamma correction and contrast enhancement. Initially, MA detection was performed using a modified double ring filter, which provides MA along with blood vessels. Further, the vessels were removed using original double ring filter. The results of these five MA detection methods were evaluated using ROC. Ok Medical [138] outperformed all other methods and human expert. Their method obtained an area under ROC of 0.89. The summary of the MA and HEM segmentation methods is presented in Table 6.

3.6. Detection of macular edema

DME is a complication of DR particularly in aged Type-2 diabetes patients [21]. It causes loss of visual acuity and also affects the central vision of the diabetes patients having early sign of DR [140]. It is mainly classified into two types viz., Clinically Significant Macular Edema (CSME) and Non Clinically Significant Macular Edema (NCSME). CSME occurs if there is thickening at the center of macula, or presence of hard exudates within 500 μ m

of radius around macula [21]. DME can be clinically evaluated using stereoscopic fundus photographs and slit-lamp fundus stereo biomicroscopy [140]. The results are subjective and mainly depends on experience of the clinicians. Very few [16,141] methods are available to automatically diagnose DME. However, several authors have analyzed retinal thickening using OCT and proved that OCT imaging is a precise and reliable method to evaluate macular edema [140,142].

Giancardo et al. [16] have proposed an exudate-based DME detection method using retinal fundus images. During preprocessing the green plane image was subjected to morphological reconstruction for contrast normalization. Further, the exudate candidate was selected using hard threshold method. The 8-neighborhood connected component analysis was performed on these exudate candidates. Next, exudate edge values were compared with the Kirsch's edges of non-exudate structures. The features based on color, and wavelet were extracted. These features were fed to the k-NN, Naive Bayes, SVM and Random forests classifiers to identify the DME. They evaluated their algorithm with MESSIDOR dataset. Their algorithm obtained an area under ROC of 0.94 using SVM classifier.

Phillips et al. [141] have developed fundus imaging and processing system to quantify ME, exudates, and MA in DR. Initially, color slides or Fluorescein Angiography (FA) negatives were used for imaging. The square shape mask was used to quantify the fluorescence intensity gradient in the foveal region. Further, exudates were detected around the macular area using illumination correction, contrast enhancement and thresholding. MA were segmented and counted around the macular region using shade correction, matched filtering and shape operators. The accuracy of the macular leakage techniques was approximately 97%.

Nayak et al. [143] have developed an automated classification strategy to discriminate normal, CSME and NCSME fundus images using exudate-based features and NN. During preprocessing the color normalization was performed using histogram specification and contrast enhancement using locally adaptive transformation. The OD was recognized using variance of intensity of adjacent pixels. The positional constraint and intensity-hue-saturation transformation was used to locate the fovea. Morphological operations and thresholding was performed to detect the exudates. The location of exudates and area of exudates in the foveola, fovea, parafovea and perifovea regions were extracted. These features were fed to the NN model to discriminate normal, CSME and NCSME. Their method showed a detection sensitivity of 95.4% and specificity of 100%.

Sadda et al. [144] have compared the performance of OCT grid scanning protocol and biomicroscopic examination for the detection of CSME. Forty DME patients underwent OCT using both Macular Grid5 scanning protocol and Fast Macular Thickness Map. An automated image processing algorithm was developed based on ETDRS protocol for the Macular Grid5 scan data to plot retinal thickness, area of edema and distance from macula. These results were compared with the clinical examination and stereo fundus imaging. They showed that, Macular Grid5 scan method obtained a sensitivity of 89% and specificity of 86% for the detection of CSME.

Strøm et al. [145] have compared retinal thickening in DME using Stereoscopic Fundus Photographs (SFPs) and OCT imaging methods. The SFP and OCT images of 84 eyes were compared using location and area of retinal thickening. Further, retinal thickness was mapped topographically and the subjective thickness map was overlaid. The location of the retinal thickening was evaluated using degree of agreement. Exact agreement on area was identified in 69 (84.1%) of 82 eyes.

Kim et al. [146] have analyzed the patterns of morphological changes in DME using OCT. They performed retrospective study of DME patients. The OCT images were analyzed for the presence of diffuse retinal thickening, cystoid macular edema, posterior

Table 6

Literature review of segmentation of MA and HEM.

Authors	Methods (dataset size)	Salient feature	Performance measure
Segmentation of MA			
Spencer et al. [125]	Morphological methods and matched filter (Not Available (NA))	Region growing	Sensitivity-82%, specificity-86%
Cree et al. [126]	Peak of correlation function and region growing (20)	Shape, intensity, and rule based classifier combination	Sensitivity-82%, specificity-84%
Frame et al. [120]	Matched filter, region growing, LDA, NN and Rule based method (68)	Circularity and grayscale intensity used to detect MA	Sensitivity-84%, specificity-85%
Hansgen et al. [124]	Matched filter, region growing and Peak of correlation function (3)	Matched filter and region growing used to detect MA	Sensitivity-95.30% (DWT), sensitivity-93.60% (JPEG)
Hipwell et al. [133]	Size and shape (3783)	Rule based classifier	Sensitivity-81%, specificity-93%
Sinthanayothin [113]	RRGT and moat operator (30)	Moat operator sharpen the red lesion edges	Sensitivity-77.50%, specificity-88.70%
Streeter and Cree [129]	Top-hat, matched filter and region growing (20)	Can detect MA with greater than ten pixels	Sensitivity-56%
Larsen et al. [131]	Size and shape (200)	RetinaLyze System	Red lesion detection specificity-71.4%
Usher et al. [31]	RRGT and moat operator (1273)	Moat operator sharpen the red lesion edges	Sensitivity-95.10%, specificity-46.30%
Niemeijer [117]	Pixel classification using k-NN (140)	Performs well with pixel similarity, color, first and second order Gaussian filters	Sensitivity-100%, specificity-87%
Fleming et al. [35]	Contrast normalization and watershed retinal region growing method (1441)	Contrast normalization discriminate MA and dots	Sensitivity-85.40%, specificity-83.10%
Walter et al. [121]	Gaussian filtering, top-hat (94)	Kernel density estimation with variable bandwidth	Sensitivity-88.5%
Hatanaka et al. [122]	Brightness correction and thresholding (125)	False Positive (FP) elimination in the non-contrast images	Sensitivity-80%, specificity-88%
Quellec et al. [123]	Optimal wavelet transform (120)	Automated selection of wavelet basis, subbands, and template-matching parameter	Sensitivity-89.62% (color), 90.24% (green filtered) and 93.74% (angiographs), specificity-89.50% (color), 89.75% (green filtered) and 91.67% (angiographs)
Zhang et al. [128]	Multi-scale correlation filtering and dynamic thresholding (89)	Automated selection of kernel sigma value to detect MA	Sensitivity-71.30%
Antal and Hajdu [134]	Ensemble-based system (1200)	High flexibility for different datasets	AUC-0.90
Lazar and Hajdu [130]	Directional cross-section profile features (60)	Able to distinguish blood vessel bifurcation and crossings from MA	ROC score-0.423
Segmentation of HEM			
Gardner [116]	NN (301)	Statistical threshold tuning	Sensitivity-73.80%
Zhang and Chutatape [132]	PCA and SVM (30)	Use of rotation and illumination invariance	TPR-89.10%
Fleming et al. [34]	Multi-scale, morphological technique and SVM (10846)	Discontinuity assessment method	Sensitivity-98.60%, specificity-95.50%

hyaloidal traction, serous retinal detachment, traction retinal detachment, retinal thickening and visual acuity. Their results revealed a strong correlation between retinal thickness and visual acuity.

Sánchez-Tocino et al. [147] have assessed the retinal thickness of diabetes patients using OCT. The retinal thickness was analyzed from control, patients with NPDR without CSME, PDR without CSME, and PDR with CSME groups. The results show a significant difference in foveal thickness between control and diseased groups. The foveal thickening measured by OCT is useful in early detection of DME.

The topography of macular thickening in DME was analyzed using OCT [148]. Totally, 182 eyes of 107 patients with DR, 55 eyes from 31 patients with diabetes without retinopathy and 73 eyes from 41 control subjects were studied. The radial spoke pattern OCT imaging was performed on fovea. Retinal thickness was computed automatically from the tomograms. The average thickness (*mean ± standard deviation*) of normal eyes was $174 \pm 18 \mu\text{m}$, diabetes eyes without retinopathy was $174 \pm 17 \mu\text{m}$ and eyes with NPDR was $256 \pm 114 \mu\text{m}$. The results shows that OCT is useful in quantifying retinal thickening in patients with DME.

Neubauer et al. [149] have compared the fluorescein leakage pattern, retinal thickness obtained using Retinal Thickness Analyzer (RTA), and OCT of DME. The study includes 30 eye images from 30 patients with DME. Initially, the FA was analyzed for 10 sub-fields to identify the source of leakage and then retinal thickness

was measured using RTA and OCT. The amount of leakage was significantly correlated with the topography of retinal thickness.

4. Computer aided diagnosis of diabetic retinopathy

In the past ten years, numerous research work was conducted in the development of automated DR diagnosis. It helps in mass eye screening of diabetic patients efficiently at a faster rate. Fig. 6 depicts the overall approach of the CAD system. In the off-line system, a set of training images were preprocessed to extract features. Further, significant features were selected using filtering or wrapper methods [150,151] and used to train the classifier. In the on-line system, only the significant features which were selected during training phase were extracted from the testing set. The trained model classifies the test set into either normal or DR class using the significant features. Further, the classifier performance was evaluated by comparing the predicted and gold standard labels of the test set, which provides the accuracy, sensitivity, and specificity. This section describes systematic survey of automatic diagnosis of DR using retinal fundus images. The aim of the CAD is to distinguish normal and DR using features like area of MA, exudates, blood vessels, node points, HEM, textures, etc. Table 7 summarizes the automated DR classification systems available in the literatures.

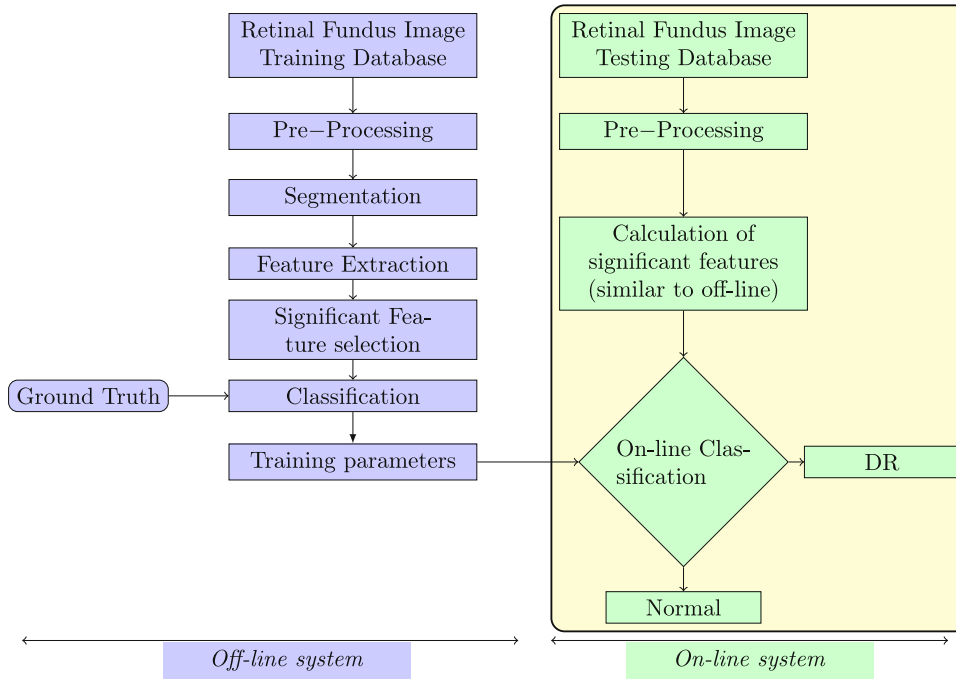


Fig. 6. Overview of the computational steps in automated DR diagnosis.

Two-class (normal and DR) classification: Screening tool for DR was developed by (Usher et al. [31], Sinthanayothin et al. [30], Aptel et al. [152], Reza and Eswaran [7], Garner et al. [116], Kahai et al. [153], Osareh et al. [154], and Quellec et al. [33]) using clinical features namely blood vessels, exudates, CWS, MA, and HEM. Exudates were extracted using RRGT and adaptive intensity thresholding [31] and dark lesions were extracted using moat operator [31]. Quellec et al. [33] have used optimal filters to segment out MA. The ANN [31,30,116] and Bayesian frame work [153] were used to classify the lesions. Their algorithm yielded a sensitivity of 95.1%, and specificity of 46.3% [31]. Sinthanayothin et al. [30] have proposed an automated DR detection system using morphological features. Initially, the retinal images were preprocessed using adaptive local contrast enhancement. Further, the OD, blood vessels were identified using intensity variation and NN. The hard exudates were identified using RRGT. The MA and HEM were identified using intensity information. Finally, all these features were combined and fed to NN classifier to detect DR. Their method obtained a sensitivity of 80.21% and specificity of 70.66%. Aptel et al. [152] have experimented the effect of field number (single or three) and mydriasis or non-mydriasis in digital fundus photography for screening of DR. Their methods obtained a kappa value of 0.82, 0.90, 0.90 and 0.95, respectively. Reza and Eswaran [7] reported an accuracy of 97% for the detection of bright lesion using rule based classification. Garner et al. [116] have proposed an automated DR detection using pixel intensity and ANN. Their method obtained a sensitivity of 88.4% and specificity of 83.5%. Kahai et al. [153] have used morphological features for automated DR detection and reported a sensitivity of 100% and specificity of 67%. Osareh et al. [154] have classified the two classes using FCM with an accuracy of 90.1%. Moreover, optimal filter frame work [33] using wavelet was able to classify DR lesions with AUC of 0.927. These above discussed DR detection systems have reported less specificity. However, their performance can be increased further by using more images and better features.

The automated telescreening system was introduced by Neubauer et al. and Suthammanas et al. [155,29] using RTA and exudates. They reported a mean sensitivity of 93% for PDR using RTA. In another

study [29] exudates were detected with an accuracy of 92.52%. However, this system used only RTA and exudate features for classification.

Larsen et al. [156] have demonstrated an automatic detection of DR in fundus photographs using visibility threshold. Their system was able to identify patients with DR and without DR with an accuracy of 90.1% and 81.3% correctly. This system separated patients with diabetes in addition to DR.

Aguro et al. [157] have used multiscale Amplitude Modulation (AM)-Frequency Modulation (FM) based decomposition to discriminate normal and DR images. Texture features namely instant amplitude, magnitude of frequency and relative frequency angle with different scales obtained from MESSIDOR database were used and reported an area under ROC of 0.98.

Wavelet transform coupled with SVM has yielded an accuracy of 99.17% in classifying two classes [158]. Moreover, they introduced Diabetic Retinopathy Risk Index (DRRI) to diagnose two groups.

Jelinek et al. [159] have proposed an automated DR detection based on MA. Their MA detection system based on Spencer [125] and Cree [126] system achieved a sensitivity of 85% and specificity of 90%.

Hansen et al. [160] have proposed an automated DR screening method using red lesions. Their method was based on Larsen et al. [156,131] red lesion detection method and reported a sensitivity of 100% with and without pupil dilation.

Brâmoff et al. [161] have developed an algorithm called Eye-Check for automated DR detection. Their algorithm was able to detect abnormal lesions such as MA, HEM, exudates, and CWS with an AUC of 0.839.

Dupas et al. [162] have developed an CAD system for grading DR. The features such as MA, HEM, exudates were used to design the classifier model. Features coupled with k-NN classifier was able to detect DR with a sensitivity of 83.9% and specificity of 72.7%.

Three-class (normal, NPDR and PDR) classification: Three classes were classified using HEM and MA, hard exudates, and CWS [163]. This method was accurate in classifying the mild, moderate, and severe NPDR stages with an accuracy of 82.6%, 82.6%, and 88.3% respectively.

Table 7
Automated DR detection methods.

Authors	Features	Methods (Dataset size)	Salient feature	Performance measure
Two class classification				
Garner et al. [116]	Pixel intensity	NN (301)	Statistical threshold tuning	Sensitivity-88.40%, specificity-83.50%
Osareh et al. [154]	HEM, MA, hard exudates and cottonwool spots	FCM (142)	Precisely detect's exudates	Accuracy-90.10%
Larsen et al. [156]	Red lesions	DR Visibility threshold (260)	Adjustable visibility thresholding	Sensitivity-96.70%, specificity-71.40%
Sinthanayothin et al. [30]	HEM, MA, and hard exudates	NN (767)	Real time screening	Sensitivity-80.21%, specificity-70.66%
Hansen et al. [160]	Red lesions	DR Visibility threshold (83)	With and without pupil dilation	Sensitivity-97%, specificity-75%
Usher et al. [31]	HEM, MA, hard exudates and cottonwool spots	NN (1273)	Detects maculopathy also	Sensitivity-95.10%, specificity-46.30%
Abramoff et al. [27]	Web-based questionnaire, visual acuity measurement	EyeCheck software (1676)	Telediagnosis system	Interrater agreement-0.93
Neubauer et al. [155]	Retinal thickness	RTA (61)	RTA used for telescreening of DR	Sensitivity-93% (PDR)
Jelinek et al. [159]	MA	Waikato automated MA detector (543)	Color non-mydiatic images can be analyzed	Sensitivity-85%, specificity-90%
Kahai et al. [153]	MA	statistical learning (143)	Less computational time (10 ns)	Sensitivity-100%, specificity-67%
Philip et al. [19]	MA and HEM	Wilson score and kappa statistic (527)	Adaptable to local imaging methods and equipments	Accuracy-99.1%
Aptel et al. [152]	HEM, MA, hard exudates and cottonwool spots	Kappa analysis (158)	Three-field strategy without pupil dilation	Degree of agreement-0.82 (single), 0.90 (three), 0.90 (mydriasis), 0.95 (non-mydriasis)
Suthammanas et al. [29]	Exudates	DR telescreening system (100)	Can handle images from various hospitals	Accuracy-92.52%
Agurto et al. [157]	AM-FM features	Distance metrics (376)	Rapid retraining	ROC-0.98
Abràmoff et al. [161]	MA, HEM, exudates, and CWS	k-NN classifier (16,770)	It can discard poor quality images	AUC-0.839
Dupas et al. [162]	MA, HEM, and exudates	k-NN classifier (761)	It can able to detect ME	Sensitivity-83.9%, specificity-72.7%
Quellec et al. [33]	Optimal filter frame work	k-NN (67)	Detects drusen and Stargardt's disease flecks also	AUC-0.927
Reza and Eswaran [7]	Hard exudates, CWS, and large plaque of hard exudates	Rule based classifier (20)	Accurate grading of NPDR lesions	Accuracy-97%
Kevin Noronha et al. [158]	Wavelet energy features	SVM (240)	DRRI	Accuracy-99.17%, sensitivity-99.17%, specificity-99.17%
Three class classification				
Lee et al. [163]	HEM, MA, exudates and CWS	NN (430)	High reproducibility	Normal-82.60% Non-Proliferative Diabetic Retinopathy-82.60% Proliferative Diabetic Retinopathy-88.30%
Nayak et al. [3]	Exudates, area of bloodvessel, and contrast	NN (140)	Texture and morphological features	Sensitivity-90% Specificity-100% Accuracy-93%
Mookiah et al. [80]	Blood vessels and exudates area, bifurcation points, global texture and entropies	GA optimized PNN classifier (156)	PNN tuning by GA and Particle Swarm Optimization (PSO)	Sensitivity-96.27%, specificity-96.08%, accuracy-96.15%
Four class classification				
Yun et al. [164]	Perimeter of the blood vessels	NN (124)	Morphological features	Sensitivity-90%, specificity-100%, accuracy-84%
Acharya et al. [165]	Co-occurrence matrix and run length matrix	SVM (238)	DRRI	Sensitivity-98.9%, specificity-89.5%, accuracy-100%
Five class classification				
Acharya et al. [166]	Higher Order Spectra (HOS)	SVM (300)	Non-linear features	Sensitivity-82.50%, specificity-88.90%, accuracy-82%
Acharya et al. [167]	Blood vessel area, exudates, MA, and MA	SVM (331)	Morphological features	Sensitivity-82%, specificity-86%, accuracy-85.9%

Nayak et al. [3] have used features like blood vessels, exudates and texture and classified with an average accuracy of 93%, sensitivity of 90%, and specificity of 100% using NN.

Mookiah et al. [80] have used features like blood vessels area, bifurcation (node) points in the blood vessels, exudates area, texture and entropies. Their results shows that the GA optimized Probabilistic Neural Network (PNN) classifier was able to identify normal class correctly with an accuracy of 92.88% NPDR and PDR with 96.97% and 100% respectively. The sensitivity and specificity of their system was 96.27% and 96.08% respectively.

Four-class (normal, moderate NPDR, severe NPDR and PDR) classification: Yun et al. [164] have used blood vessel area and perimeter coupled with NN and reported an average accuracy of 84%, sensitivity and specificity of 90% and 100% respectively.

Acharya et al. [165] have proposed an automated DR detection system using texture and presented an accuracy of 85.2%, sensitivity of 98.9% and specificity of 89.5%. The authors also proposed a DR index using the combination of texture features, which was able to identify the different stages of DR and ME.

Five-class (normal, mild DR, moderate DR, severe DR, and PDR) classification: Acharya et al. [166] have automatically classified five classes using the bispectral invariant features of HOS techniques and an SVM classifier. They reported an average accuracy of 82%, sensitivity of 82% and specificity of 88%.

Same group [167] have used the blood vessels, exudates, MA, and HEM features coupled with SVM classifier and demonstrated a classification accuracy of 85%, sensitivity of 82%, and specificity of 86%.

5. Summary

This review presents a detailed survey of algorithms and results used for the automated identification of DR stages using fundus photographs. The robust DR mass screening tool will significantly reduce the workload of ophthalmologists and graders in clinics. The process of analysing retinal images involves series of steps namely identifying the anatomical structure, extracting pathological lesions, feature extraction and classification. All these steps involve various techniques or algorithms. Initially, the overall performance of the anatomy and pathology detection algorithms were evaluated quantitatively. Further, individual steps of these algorithms were evaluated to achieve higher performance [38]. Even though significant achievements have been made in digital fundus image analysis, challenges still exists in the selection of best algorithms which yields higher accuracy during DR screening.

For the detection of anatomical structures in the retinal images, intensity and NN based methods have performed effectively [50]. The blood vessel extraction results of Chaudhuri et al. [48], and Hoover et al. [79] have reported good results using standard dataset. However, the automated analysis of retinal images are affected by image quality, laser scars and noise [168]. The important problem in the automated segmentation of basic structures (OD, blood vessels and fovea) and abnormal lesions (exudates, MA, and HEM) is obtaining the ground-truth.

Several studies reported different novel algorithms to detect the various salient features of the retina. The abnormalities present at fovea have higher clinical significance than at other regions. Moreover, organized standard research methodologies are required to evaluate the algorithms in each step and as a whole report the sensitivity and specificity. Nevertheless, the best feature extraction algorithm and robust classifier to be used to obtain the highest accuracy is still a debatable issue. The ME can be detected only with stereoscopic images or direct examination using slit-lamp biomicroscopy. Also, the drusen can be clearly detected only with stereoscopic images [41].

Few research papers [30,156,164,166,33,165] investigated automated DR detection with abnormal lesions which might need additional examination by the ophthalmologists. Moreover, any CAD system should have high specificity during screening with minimum false negatives. This will reduce the burden on the ophthalmologists by focusing only on the abnormal DR images.

Abramoff et al. [28] have suggested that the segmentation methods developed by the authors should be evaluated using open source (public) datasets. Two open source data sets such as STructured Analysis of the Retina [169] and DRIVE [170] are available with different diagnosis and facilitates to perform comparative studies in blood vessel segmentation. Moreover, DIARETDB1 [171] is a public database available for benchmarking DR detection using fundus images. The results of different methods can be compared using this dataset. They invite the research communities to evaluate their developed methods with this database and share their results on the web. Moreover, fundus image analysis of DR requires a large set of training images with various lesions that can be used by the other researchers to evaluate their proposed systems. These data sharing was initiated by approved research councils and also sponsors should support the creation of such database. Bossuyt et al. [172] presented the STAndards for the Reporting of Diagnostic accuracy studies (STARD) for analysing the performance of diagnosis tests for Diabetic Retinopathy. This procedure may be used as a standard format for reporting DR screening studies.

Finally, the CAD system performance need to be tested with best features, diverse images and robust classifiers. In addition to morphological features one can use texture features such as local binary pattern, laws mask [80] and gray co-matrix [165] and other non-linear features such as HOS and bi-spectral entropies [173] to achieve higher accuracy. Moreover, the classifier parameters can also be optimized using evolutionary algorithms to yield higher accuracy [80]. A CAD system which can detect the True Negative (TN) (normal images) correctly can significantly reduce the burden of the ophthalmologists significantly. Nowadays, authors have proposed an integrated index called DRRI computed from the clinically significant features. It is one number having unique ranges for different classes [158,165,174]. This may be used to classify the various classes and can help the doctors significantly in their DR screening [158,165].

Conflict of interest statement

I (we) certify that there is no conflict of interest with any financial organization regarding the material discussed in the paper.

Acknowledgments

Authors thank Social Innovation Research Fund (SIRF) and NHG Clinician Scientist Career Scheme (CSCS/12006) Grant, Singapore for providing financial support for this research.

References

- [1] A.A. Alghadyan, Diabetic retinopathy—an update, *Saudi J. Ophthalmol.* 25 (1) (2011) 99–111.
- [2] U.R. Acharya, O. Faust, N.A. Kadri, J.S. Suri, W. Yu, Automated identification of normal and diabetes heart rate signals using nonlinear measures, *Comput. Biol. Med.* 43 (10) (2013) 1523–1529.
- [3] J. Nayak, P. Bhat, U.R. Acharya, C.M. Lim, M. Kagathi, Automated identification of diabetic retinopathy stages using digital fundus images, *J. Med. Syst.* 32 (2008) 107–115.
- [4] F. Harney, Diabetic retinopathy, *Medicine* 34 (3) (2006) 95–98.

- [5] M.H.A. Fadzil, Lilalznita Izhar, Hermawan Nugroho, HanungAdi Nugroho, Analysis of retinal fundus images for grading of diabetic retinopathy severity, *Med. Biol. Eng. Comput.* 49 (2011) 693–700.
- [6] L. Verma, G. Prakash, H.K. Tewari, Diabetic retinopathy: time for action. No complacency please!, *Bull. W.H.O.* 80 (2002) 419.
- [7] A. Reza, C. Eswaran, A decision support system for automatic screening of non-proliferative diabetic retinopathy, *J. Med. Syst.* 35 (2011) 17–24.
- [8] S. Wild, G. Roglic, A. Green, R. Sicree, H. King, Global prevalence of diabetes: estimates for the year 2000 and projections for 2030, *Diabetes Care* 27 (5) (2004) 1047–1053.
- [9] G.G. Yen, W.-F. Leong, A sorting system for hierarchical grading of diabetic fundus images: a preliminary study, *IEEE Trans. Inf. Technol. Biomed.* 12 (1) (2008) 118–130.
- [10] R. Williams, M. Airey, H. Baxter, J. Forrester, T. Kennedy-Martin, A. Girach, Epidemiology of diabetic retinopathy and macular oedema: a systematic review, *Eye (London)* 18 (2004) 963–983.
- [11] E.T.D.R.S.R. Group, Grading diabetic retinopathy from stereoscopic color fundus photographs—an extension of the modified Airlie House classification, *Ophthalmology* 98 (10) (1991) 786–806.
- [12] D. McLeod, Why cotton wool spots should not be regarded as retinal nerve fibre layer infarcts, *Br. J. Ophthalmol.* 89 (2) (2005) 229–237.
- [13] T.Y.P. Chui, L.N. Thibos, A. Bradley, S.A. Burns, The mechanisms of vision loss associated with a cotton wool spot, *Vision Res.* 49 (23) (2009) 2826–2834.
- [14] A. Patz, Studies on retinal neovascularization, Friedenwald lecture, *Invest. Ophthalmol. Visual Sci.* 19 (10) (1980) 1133–1138.
- [15] D. Vallabha, R. Dorairaj, K. Namuduri, H. Thompson, Automated detection and classification of vascular abnormalities in diabetic retinopathy, in: Conference Record of the Thirty-Eighth Asilomar Conference on Signals, Systems and Computers, 2004, vol. 2, IEEE, 2004, pp. 1625–1629.
- [16] L. Giancardo, F. Meriaudeau, T.P. Karnowski, Y. Li, S. Garg, K.W. Tobin, E. Chaum, Exudate-based diabetic macular edema detection in fundus images using publicly available datasets, *Med. Image Anal.* 16 (1) (2012) 216–226.
- [17] R.N. Frank, Diabetic retinopathy, *N. Engl. J. Med.* 350 (1) (2004) 48–58.
- [18] E.T.D.R.S.R. Group, Classification of diabetic retinopathy from fluorescein angiograms, *Ophthalmology* 98 (11) (1991) 807–822.
- [19] S. Philip, A.D. Fleming, K.A. Goatman, S. Fonseca, P. Mcnamee, G.S. Scotland, G.J. Prescott, P.F. Sharp, J.A. Olson, The efficacy of automated “disease/no disease” grading for diabetic retinopathy in a systematic screening programme, *Br. J. Ophthalmol.* 91 (11) (2007) 1512–1517.
- [20] P.H. Scanlon, Diabetic retinopathy, *Medicine* 38 (12) (2010) 656–660.
- [21] T.A. Ciulla, A.G. Amador, B. Zinman, Diabetic retinopathy and diabetic macular edema pathophysiology, screening, and novel therapies, *Diabetes Care* 26 (9) (2003) 2653–2664.
- [22] I. Zechmeister-Koss, M. Huić, Vascular endothelial growth factor inhibitors (anti-vegf) in the management of diabetic macular oedema: a systematic review, *Br. J. Ophthalmol.* 96 (2) (2012) 167–178.
- [23] M. Parravano, F. Menchini, G. Virgili, Antiangiogenic therapy with anti-vascular endothelial growth factor modalities for diabetic macular oedema, *Cochrane Database Syst. Rev.* 4.
- [24] R. Karim, B. Tang, Use of antivascular endothelial growth factor for diabetic macular edema, *Clin. Ophthalmol.* 4 (2010) 493. (Auckland, NZ).
- [25] W. Hsu, P.M.D.S. Pallawala, M.L. Lee, K.-G.A. Eong, The role of domain knowledge in the detection of retinal hard exudates, in: IEEE Computer Society Conference on Computer Vision and Pattern Recognition, vol. 2, 2001, p. 246.
- [26] N. Patton, T.M. Aslam, T. MacGillivray, I.J. Deary, B. Dhillon, R.H. Eikelboom, K. Yugesan, I.J. Constable, Retinal image analysis: concepts, applications and potential, *Prog. Retinal Eye Res.* 25 (1) (2006) 99–127.
- [27] M.D. Abramoff, S.A. Maria, S. Schulten, Web-based screening for diabetic retinopathy in a primary care population: The eyecheck project, *Telemed. e-Health* 11 (6) (2006) 668–674.
- [28] M.D. Abramoff, M. Niemeijer, M.S.A. Suttorp-Schulthen, M.A. Viergever, S.R. Russell, B. van Ginneken, Evaluation of a system for automatic detection of diabetic retinopathy from color fundus photographs in a large population of patients with diabetes, *Diabetes Care* 31 (2) (2008) 193–198.
- [29] J. Suthammanas, K. Viriyachot, P. Tuntipark, B. Uyanonvara, K. Krairaksa, C. Duanggate, An automatic diabetic retinopathy telescreening system of Thailand, in: Proceedings of the International Symposium on Biomedical Engineering (ISBME 2008), 2008, pp. 88–92.
- [30] C. Sinthanayothin, V. Kongbunkiat, S. Phoojaruenchanachai, A. Singalavanija, Automated screening system for diabetic retinopathy, in: Proceedings of the 3rd International Symposium on Image and Signal Processing and Analysis, 2003. ISPA 2003, vol. 2, 2003, pp. 915–920.
- [31] D. Usher, M. Dumskyj, M. Himaga, T.H. Williamson, S. Nussey, J. Boyce, Automated detection of diabetic retinopathy in digital retinal images: a tool for diabetic retinopathy screening, *Diabetic Med.* 21 (1) (2004) 84–90.
- [32] M. Niemeijer, M.D. Abramoff, B. van Ginneken, Information fusion for diabetic retinopathy cad in digital color fundus photographs, *IEEE Trans. Med. Imaging* 28 (2009) 775–785.
- [33] G. Quellec, S.R. Russell, M.D. Abramoff, Optimal filter framework for automated, instantaneous detection of lesions in retinal images, *IEEE Trans. Med. Imaging* 30 (2) (2011) 523–533.
- [34] A.D. Fleming, K.A. Goatman, G.J. Williams, S. Philip, P.F. Sharp, J.A. Olson, Automated detection of blot haemorrhages as a sign of referable diabetic retinopathy, in: Proceedings of the Medical Image Understanding and Analysis (MIUA2008), 2008, pp. 235–239.
- [35] A.D. Fleming, S. Philip, K.A. Goatman, J.A. Olson, P.F. Sharp, Automated microaneurysm detection using local contrast normalization and local vessel detection, *IEEE Trans. Med. Imaging* 25 (9) (2006) 1223–1232.
- [36] N. Perumalsamy, N.M. Prasad, S. Sathya, K. Ramasamy, Software for reading and grading diabetic retinopathy: Aravind diabetic retinopathy screening 3.0, *Diabetes Care* 30 (2007) 2302–2306.
- [37] R.J. Winder, P.J. Morrow, I.N. McRitchie, J.R. Bailie, P.M. Hart, Algorithms for digital image processing in diabetic retinopathy, *Comput. Med. Imaging Graphics* 33 (8) (2009) 608–622.
- [38] T. Teng, M. Lefley, D. Claremont, Progress towards automated diabetic ocular screening: a review of image analysis and intelligent systems for diabetic retinopathy, *Med. Biol. Eng. Comput.* 40 (2002) 2–13.
- [39] M.D. Abramoff, M.K. Garvin, M. Sonka, Retinal imaging and image analysis, *IEEE Rev. Biomed. Eng.* 3 (2010) 169–208.
- [40] Fundus camera optics, Accessed: 30/11/2012. URL <http://www.opsweb.org/?page=fundusphotography>.
- [41] Fundus photography overview, Accessed: 30/11/2012. URL <http://www.opsweb.org/?page=fundusphotography>.
- [42] G.D. Joshi, J. Sivaswamy, S.R. Krishnadas, Optic disk and cup segmentation from monocular color retinal images for glaucoma assessment, *IEEE Trans. Med. Imaging* 30 (6) (2011) 1192–1205.
- [43] C. Sinthanayothin, Image Analysis for Automatic Diagnosis of Diabetic Retinopathy, Kings College London, 1999.
- [44] L. Gagnon, M. Lalonde, M. Beaulieu, M.C. Boucher, Procedure to detect anatomical structures in optical fundus images, in: Medical Imaging 2001: Image Processing, 2001.
- [45] J. Lowell, A. Hunter, D. Steel, A. Basu, R. Ryder, E. Fletcher, L. Kennedy, Optic nerve head segmentation, *IEEE Trans. Med. Imaging* 23 (2) (2004) 256–264.
- [46] L.D. Hubbard, R.J. Brothers, W.N. King, L.X. Clegg, R. Klein, L.S. Cooper, A. Sharrett, M.D. Davis, J. Cai, Methods for evaluation of retinal microvascular abnormalities associated with hypertension/sclerosis in the atherosclerosis risk in communities study, *Ophthalmology* 106 (12) (1999) 2269–2280.
- [47] M. Lalonde, L. Gagnon, M.C. Boucher, Non-recursive paired tracking for vessel extraction from retinal images, in: Proceedings of the Conference Vision Interface, 2000, pp. 61–68.
- [48] S. Chaudhuri, S. Chatterjee, N. Katz, M. Nelson, M. Goldbaum, Automatic detection of the optic nerve in retinal images, in: IEEE International Conference on Imaging Processing, 1989, pp. 1–5.
- [49] M. Goldbaum, S. Moezzi, A. Taylor, S. Chatterjee, J. Boyd, E. Hunter, R. Jain, Automated diagnosis and image understanding with object extraction, object classification, and inferencing in retinal images, in: Proceedings, International Conference on Image Processing, 1996, vol. 3, 1996, pp. 695–698.
- [50] C. Sinthanayothin, J.F. Boyce, H.L. Cook, T.H. Williamson, Automated localisation of the optic disc, fovea, and retinal blood vessels from digital colour fundus images, *Br. J. Ophthalmol.* 83 (8) (1999) 902–910.
- [51] A. Hoover, M. Goldbaum, Locating the optic nerve in a retinal image using the fuzzy convergence of the blood vessels, *IEEE Trans. Med. Imaging* 22 (8) (2003) 951–958.
- [52] T. Walter, J.C. Klein, Segmentation of color fundus images of the human retina: detection of the optic disc and the vascular tree using morphological techniques, in: J. Crespo, V. Maojo, F. Martin (Eds.), Springer, Berlin, Heidelberg, 1999.
- [53] R. Chrastek, M. Wolf, K. Donath, H. Niemann, D. Paulus, T. Hothorn, B. Lausen, R. Lammer, C.Y. Mardin, G. Michelson, Automated segmentation of the optic nerve head for diagnosis of glaucoma, *Med. Image Anal.* 9 (4) (2005) 297–314.
- [54] R.A. Abdel-Ghafar, T. Morris, Progress towards automated detection and characterization of the optic disc in glaucoma and diabetic retinopathy, *Inform. Health Soc. Care.* 32 (1) (2007) 19–25.
- [55] P. Treigys, V. Šaltenis, G. Dzemyda, V. Barzdžiukas, A. Paunksnis, Automated optic nerve disc parameterization, *Informatica* 19 (3) (2008) 403–420.
- [56] C.I. Sanchez, R. Hornero, M.I. Lopez, J. Poza, Retinal image analysis to detect and quantify lesions associated with diabetic retinopathy, in: Engineering in Medicine and Biology Society, 2004. IEMBS '04. 26th Annual International Conference of the IEEE, vol. 1, 2004, pp. 1624–1627.
- [57] H. Li, O. Chutatape, Automated feature extraction in color retinal images by a model based approach, *IEEE Trans. Biomed. Eng.* 51 (2) (2004) 246–254.
- [58] M. Lalonde, M. Beaulieu, L. Gagnon, Fast and robust optic disc detection using pyramidal decomposition and Hausdorff-based template matching, *IEEE Trans. Med. Imaging* 20 (11) (2001) 1193–1200.
- [59] M. Foracchia, E. Grisan, A. Ruggeri, Detection of optic disc in retinal images by means of a geometrical model of vessel structure, *IEEE Trans. Med. Imaging* 23 (10) (2004) 1189–1195.
- [60] A.A.H. Abdel-Razik Youssif, A.Z. Ghalwash, A.A.S. Abdel-Rahman Ghoneim, Optic disc detection from normalized digital fundus images by means of a vessels' direction matched filter, *IEEE Trans. Med. Imaging* 27 (1) (2008) 11–18.
- [61] A.D. Fleming, K.A. Goatman, S. Philip, J.A. Olson, P.F. Sharp, Automatic detection of retinal anatomy to assist diabetic retinopathy screening, *Phys. Med. Biol.* 52 (2) (2007) 331.
- [62] M. Niemeijer, M.D. Abramoff, B. van Ginneken, Segmentation of the optic disc, macula and vascular arch in fundus photographs, *IEEE Trans. Med. Imaging* 26 (1) (2007) 116–127.
- [63] F. Mendels, C. Heneghan, P.D. Harper, R.B. Reilly, J.-P. Thiran, Extraction of the optic disk boundary in digital fundus images, in: Engineering in Medicine and Biology, 1999. 21st Annual Conference and the 1999 Annual Fall Meeting of the Biomedical Engineering Society. BMES/EMBS Conference, 1999. Proceedings of the First Joint, vol. 2, 1999, p. 1139.

- [64] F. Mendels, C. Heneghan, J. Thiran, Identification of the optic disk boundary in retinal images using active contours, in: Proceedings of Irish Machine Vision and Image Processing Conference (IMVIP) 1999, Cerebrovascular Diseases, IEEE, 1999, pp. 103–115.
- [65] M. Kass, A. Witkin, D. Terzopoulos, Snakes: active contour models, *Int. J. Comput. Vision* 1 (4) (1988) 321–331.
- [66] C. Xu, J.L. Prince, Snakes, shapes, and gradient vector flow, *IEEE Trans. Image Process.* 7 (3) (1998) 359–369.
- [67] M.R.K. Mookiah, U.R. Acharya, C.K. Chua, L.C. Min, E.Y.K. Ng, M.M. Mushrif, A. Laude, Application of intuitionistic fuzzy histon segmentation for the automated detection of optic disc in digital fundus images, in: 2012 IEEE-EMBS International Conference on Biomedical and Health Informatics (BHI), 2012, pp. 444–447.
- [68] M.R.K. Mookiah, U.R. Acharya, C.K. Chua, L.C. Min, E.Y.K. Ng, M.M. Mushrif, A. Laude, Automated detection of optic disk in retinal fundus images using intuitionistic fuzzy histon segmentation, *Proc. Inst. Mech. Eng. H.J. Eng. Med.* 227 (1) (2013) 37–49.
- [69] M. Ahmad Hijazi, F. Coenen, Y. Zheng, Image classification using histograms and time series analysis: a study of age-related macular degeneration screening in retinal image data, in: P. Perner (Ed.), *Advances in Data Mining. Applications and Theoretical Aspects*, Lecture Notes in Computer Science, vol. 6171, Springer, Berlin, Heidelberg, 2010, pp. 197–209.
- [70] S. Chaudhuri, S. Chatterjee, N. Katz, M. Nelson, M. Goldbaum, Detection of blood vessels in retinal images using two-dimensional matched filters, *IEEE Trans. Med. Imaging* 8 (3) (1989) 263–269.
- [71] S.S. Lee, M. Rajeswari, D. Ramachandram, B. Shaharuddin, Screening of diabetic retinopathy—automatic segmentation of optic disc in colour fundus images, in: The 2nd International Conference on Distributed Frameworks for Multimedia Applications, 2006, pp. 1–7.
- [72] Y.A. Tolias, S.M. Panas, A fuzzy vessel tracking algorithm for retinal images based on fuzzy clustering, *IEEE Trans. Med. Imaging* 17 (2) (1998) 263–273.
- [73] K.-H. Englmeier, K. Schmid, C. Hildebrand, S. Bichler, M. Porta, M. Maurino, T. Bek, Early detection of diabetes retinopathy by new algorithms for automatic recognition of vascular changes, *Eur. J. Med.* 9 (2004) 473–478.
- [74] M. Vlachos, E. Dermatas, Multi-scale retinal vessel segmentation using line tracking, *Comput. Med. Imag. Grap.* 34 (3) (2010) 213–227.
- [75] B. Nayebifar, H.A. Moghaddam, A novel method for retinal vessel tracking using particle filters, *Comput. Biol. Med.* 43 (5) (2013) 541–548.
- [76] F. Zana, J.-C. Klein, Segmentation of vessel-like patterns using mathematical morphology and curvature evaluation, *IEEE Trans. Image Process.* 10 (7) (2001) 1010–1019.
- [77] M. Al-Rawi, H. Karajeh, Genetic algorithm matched filter optimization for automated detection of blood vessels from digital retinal images, *Comput. Methods Prog. Biomed.* 87 (3) (2007) 248–253.
- [78] A. Osareh, B. Shadgar, Automatic blood vessel segmentation in color images of retina, *Iran. J. Sci. Technol. Trans. B Eng.* 33 (2) (2009) 191–206.
- [79] A.D. Hoover, V. Kouznetsova, M. Goldbaum, Locating blood vessels in retinal images by piecewise threshold probing of a matched filter response, *IEEE Trans. Med. Imaging* 19 (3) (2000) 203–210.
- [80] M.R.K. Mookiah, U.R. Acharya, R.J. Martis, C.K. Chua, L.C. Min, E.Y.K. Ng, A. Laude, Evolutionary algorithm based classifier parameter tuning for automatic diabetic retinopathy grading: a hybrid feature extraction approach, *Knowl. Based Syst.* 39 (0) (2013) 9–22.
- [81] L. Gangand, O. Chutatapeand, E. Al, Detection and measurement of retinal vessels in fundus images using amplitude modified second-order Gaussian filter, *IEEE Trans. Biomed. Eng.* 49 (2) (2002) 168–172.
- [82] B. Zhang, L. Zhang, L. Zhang, F. Karray, Retinal vessel extraction by matched filter with first-order derivative of Gaussian, *Comput. Biol. Med.* 40 (4) (2010) 438–445.
- [83] L. Zhang, Q. Li, J. You, D. Zhang, A modified matched filter with double-sided thresholding for screening proliferative diabetic retinopathy, *IEEE Trans. Inf. Technol. Biomed.* 13 (4) (2009) 528–534.
- [84] H. Li, W. Hsu, M.-L. Lee, H. Wang, A piecewise Gaussian model for profiling and differentiating retinal vessels, in: Proceedings. 2003 International Conference on Image Processing, 2003. ICIP 2003, vol. 1, IEEE, 2003, pp. I–1069.
- [85] D. Wu, M. Zhang, J.-C. Liu, W. Bauman, On the adaptive detection of blood vessels in retinal images, *IEEE Trans. Biomed. Eng.* 53 (2) (2006) 341–343.
- [86] M. Niemeijer, J. Staal, B. van Ginneken, M. Loog, M.D. Abramoff, Comparative study of retinal vessel segmentation methods on a new publicly available database, in: Medical Imaging 2004, International Society for Optics and Photonics, 2004, pp. 648–656.
- [87] B.S. Lam, Y. Gao, A.W. Liew, General retinal vessel segmentation using regularization-based multiconcavity modeling, *IEEE Trans. Med. Imaging* 29 (2010) 1369–1381.
- [88] K.A. Goatman, A.D. Fleming, S. Philip, G.J. Williams, J.A. Olson, P.F. Sharp, Detection of new vessels on the optic disc using retinal photographs, *IEEE Trans. Med. Imaging* 30 (4) (2011) 972–979.
- [89] F. Meyer, Topographic distance and watershed lines, *Signal Process.* 38 (1) (1994) 113–125.
- [90] M.E. Martinez-Perez, A.D. Hughes, S.A. Thom, A.A. Bharath, K.H. Parker, Segmentation of blood vessels from red-free and fluorescein retinal images, *Med. Image Anal.* 11 (1) (2007) 47–61.
- [91] A. Hunter, J. Lowell, D. Steel, A. Basu, R. Ryder, Non-Linear Filtering for Vascular Segmentation and Detection of Venous Beading, University of Durham, 2002.
- [92] B. Al-Diri, A. Hunter, D. Steel, An active contour model for segmenting and measuring retinal vessels, *IEEE Trans. Med. Imaging* 28 (9) (2009) 1488–1497.
- [93] J. Staal, M.D. Abramoff, M. Niemeijer, M.A. Viergever, B. Van Ginneken, Ridge-based vessel segmentation in color images of the retina, *IEEE Trans. Med. Imaging* 23 (2004) 501–509.
- [94] J.V.B. Soares, J.J.G. Le, R.M. Cesar, H.F. Jelinek, M.J. Cree, S. Member, Retinal vessel segmentation using the 2-d Gabor wavelet and supervised classification, *IEEE Trans. Med. Imaging* 25 (2006) 1214–1222.
- [95] D. Marin, A. Aquino, M.E. Gegundez-Arias, J.M. Bravo, A new supervised method for blood vessel segmentation in retinal images by using gray-level and moment invariants-based features, *IEEE Trans. Med. Imaging* 30 (1) (2011) 146–158.
- [96] E. Ricci, R. Perfetti, Retinal blood vessel segmentation using line operators and support vector classification, *IEEE Trans. Med. Imaging* 26 (2007) 1357–1365.
- [97] F. Rossant, M. Badellino, A. Chavillon, I. Bloch, M. Paques, A morphological approach for vessel segmentation in eye fundus images, with quantitative evaluation, *J. Med. Imaging Health Inf.* 1 (1) (2011) 42–49.
- [98] M.H.A. Fadil, L.I. Izhar, H.A. Nugroho, Determination of foveal avascular zone in diabetic retinopathy digital fundus images, *Comput. Biol. Med.* 40 (7) (2010) 657–664.
- [99] U.R. Acharya, E.Y.K. Ng, J.S. Suri, *Image Modeling of the Human Eye*, Artech House, 2008.
- [100] H. Narasimha-Iyer, A. Can, B. Roysam, H.L. Tanenbaum, A. Majerovics, Integrated analysis of vascular and nonvascular changes from color retinal fundus image sequences, *IEEE Trans. Biomed. Eng.* 54 (8) (2007) 1436–1445.
- [101] K. Goatman, A. Charnley, L. Webster, S. Nussey, Assessment of automated disease detection in diabetic retinopathy screening using two-field photography, *PLoS ONE* 6 (12) (2011) e27524.
- [102] C. Köse, U. Şevik, O. Gencalioğlu, Automatic segmentation of age-related macular degeneration in retinal fundus images, *Comput. Biol. Med.* 38 (5) (2008) 611–619.
- [103] K.W. Tobin, E. Chaum, V.P. Govindasamy, T.P. Karnowski, Detection of anatomic structures in human retinal imagery, *IEEE Trans. Med. Imaging* 26 (12) (2007) 1729–1739.
- [104] A. Osareh, M. Mirmehdi, B. Thomas, R. Markham, Automated identification of diabetic retinal exudates in digital colour images, *Br. J. Ophthalmol.* 87 (2003) 1220–1223.
- [105] A. Osareh, B. Shadgar, R. Markham, A computational-intelligence-based approach for detection of exudates in diabetic retinopathy images, *IEEE Trans. Inf. Technol. Biomed.* 13 (4) (2009) 535–545.
- [106] A. Sopharak, B. Uyyanonvara, S. Barman, Automatic exudate detection for diabetic retinopathy screening, *ScienceAsia* 35 (2009) 80–88.
- [107] J.C. Dunn, A fuzzy relative of the isodata process and its use in detecting compact well-separated clusters, *J. Cybern.* 3 (3) (1973) 32–57.
- [108] J.C. Bezdek, *Pattern Recognition with Fuzzy Objective Function Algorithms*, Plenum, New York, NY, USA, 1981.
- [109] A. Sopharak, K. That New, Y.N. Aye Moe, M. Dailey, B. Uyyanonvara, Automatic exudate detection with a naive Bayes classifier, in: International Conference on Embedded Systems and Intelligent Technology, 2008, pp. 139–142.
- [110] A. Sopharak, B. Uyyanonvara, S. Barman, T.H. Williamson, Automatic detection of diabetic retinopathy exudates from non-dilated retinal images using mathematical morphology methods, *Comput. Med. Imaging Graphics* 32 (8) (2008) 720–727.
- [111] T. Walter, J.-C. Klein, P. Massin, A. Erginay, A contribution of image processing to the diagnosis of diabetic retinopathy—detection of exudates in color fundus images of the human retina, *IEEE Trans. Med. Imaging* 21 (10) (2002) 1236–1243.
- [112] C.I. Sanchez, M. Garcia, A. Mayo, M.I. Lopez, R. Hornero, Retinal image analysis based on mixture models to detect hard exudates, *Med. Image Anal.* 13 (4) (2009) 650–658.
- [113] C. Sinthanayothin, J.F. Boyce, T.H. Williamson, H.L. Cook, E. Mensah, S. Lal, D. Usher, Automated detection of diabetic retinopathy on digital fundus images, *Diabetic Med.* 19 (2) (2002) 105–112.
- [114] A.D. Fleming, S. Philip, K.A. Goatman, G.J. Williams, J.A. Olson, P.F. Sharp, Automated detection of exudates for diabetic retinopathy screening, *Phys. Med. Biol.* 52 (24) (2007) 7385.
- [115] D. Welfer, J. Scharcanski, D.R. Marinho, A coarse-to-fine strategy for automatically detecting exudates in color eye fundus images, *Comput. Med. Imaging Graphics* 34 (3) (2010) 228–235.
- [116] G.G. Gardner, D. Keating, T.H. Williamson, A.T. Elliott, Automatic detection of diabetic retinopathy using an artificial neural network: a screening tool, *Br. J. Ophthalmol.* 80 (1996) 940–944.
- [117] M. Niemeijer, B. van Ginneken, J. Staal, M.S.A. Suttorp-Schulten, M.D. Abramoff, Automatic detection of red lesions in digital color fundus photographs, *IEEE Trans. Med. Imaging* 24 (5) (2005) 584–592.
- [118] C.I. Sanchez, R. Hornero, M.I. Lopez, M. Aboy, J. Poza, D. Abasolo, A novel automatic image processing algorithm for detection of hard exudates based on retinal image analysis, *Med. Eng. Phys.* 30 (3) (2008) 350–357.
- [119] M. Niemeijer, B. van Ginneken, S.R. Russell, M.S.A. Suttorp-Schulten, M.D. Abramoff, Automated detection and differentiation of drusen, exudates and cotton-wool spots in digital color fundus photographs for diabetic retinopathy diagnosis, *Invest. Ophthalmol. Visual Sci.* 48 (5) (2007) 2260–2267.
- [120] A.J. Frame, P.E. Undrill, M.J. Cree, J.A. Olson, K.C. McHardy, P.F. Sharp, J.V. Forrester, A comparison of computer based classification methods

- applied to the detection of microaneurysms in ophthalmic fluorescein angiograms, *Comput. Biol. Med.* 28 (3) (1998) 225–238.
- [121] T. Walter, P. Massin, A. Erginay, R. Ordóñez, C. Jeulin, J.-C. Klein, Automatic detection of microaneurysms in color fundus images, *Med. Image Anal.* 11 (6) (2007) 555–566.
- [122] Y. Hatanaka, T. Nakagawa, Y. Hayashi, M. Kakogawa, A. Sawada, K. Kawase, T. Hara, H. Fujita, Improvement of automatic hemorrhages detection methods using brightness correction on fundus images, in: Proceedings of the SPIE, vol. 6915, 2008, pp. 69153E–1.
- [123] G. Quellec, M. Lamard, P.M. Josselin, G. Cazuguel, B. Cochener, C. Roux, Optimal wavelet transform for the detection of microaneurysms in retina photographs, *IEEE Trans. Med. Imaging* 27 (9) (2008) 1230–1241.
- [124] P. Hansgen, P.E. Undrill, M.J. Cree, The application of wavelets to retinal image compression and its effect on automatic microaneurysm analysis, *Comput. Methods Programs Biomed.* 56 (1) (1998) 1–10.
- [125] T. Spencer, J.A. Olson, K.C. McHardy, P.F. Sharp, J.V. Forrester, An image-processing strategy for the segmentation and quantification of microaneurysms in fluorescein angiograms of the ocular fundus, *Comput. Biomed. Res.* 29 (4) (1996) 284–302.
- [126] M.J. Cree, J.A. Olson, K.C. McHardy, J.V. Forrester, P.F. Sharp, Automated microaneurysm detection, in: Proceedings, International Conference on Image Processing, 1996, vol. 3, 1996, pp. 699–702.
- [127] M.J. Cree, J.A. Olson, K.C. McHardy, P.F. Sharp, J.V. Forrester, A fully automated comparative microaneurysm digital detection system, *Eye (Lond.)* 11 (5) (1997) 622–628.
- [128] B. Zhang, X. Wu, J. You, Q. Li, F. Karray, Detection of microaneurysms using multiscale correlation coefficients, *Pattern Recognition* 43 (6) (2010) 2237–2248.
- [129] L. Streeter, M.J. Cree, Microaneurysm detection in colour fundus images, *Image Vision Comput. New Zealand* (2003) 280–284.
- [130] I. Lazar, A. Hajdu, Retinal microaneurysm detection through local rotating cross-section profile analysis, *IEEE Trans. Med. Imaging* 32 (2) (2013) 400–407.
- [131] M. Larsen, J. Godt, N. Larsen, H. Lund-Andersen, A.K. Sjølie, E. Agardh, H. Kalm, M. Grunkin, D.R. Owens, Automated detection of fundus photographic red lesions in diabetic retinopathy, *Invest. Ophthalmol. Visual Sci.* 44 (2) (2003) 761–766.
- [132] X. Zhang, O. Chutatape, A SVM approach for detection of hemorrhages in background diabetic retinopathy, in: Proceedings. 2005 IEEE International Joint Conference on Neural Networks, 2005. IJCNN '05, vol. 4, 2005, pp. 2435–2440.
- [133] J.H. Hipwell, F. Strachan, J.A. Olson, K.C. McHardy, P.F. Sharp, J.V. Forrester, Automated detection of microaneurysms in digital red-free photographs: a diabetic retinopathy screening tool, *Diabetic Med.* 17 (8) (2000) 588–594.
- [134] B. Antal, A. Hajdu, An ensemble-based system for microaneurysm detection and diabetic retinopathy grading, *IEEE Trans. Biomed. Eng.* 59 (6) (2012) 1720–1726.
- [135] M. Niemeijer, B. van Ginneken, M.J. Cree, A. Mizutani, G. Quellec, C.I. Sanchez, B. Zhang, R. Hornero, M. Lamard, C. Muramatsu, X. Wu, G. Cazuguel, J. You, A. Mayo, Q. Li, Y. Hatanaka, B. Cochener, C. Roux, F. Karray, M. Garcia, H. Fujita, M.D. Abramoff, Retinopathy online challenge: automatic detection of microaneurysms in digital color fundus photographs, *IEEE Trans. Med. Imaging* 29 (1) (2010) 185–195.
- [136] C.I. Sánchez, R. Hornero, A. Mayo, M. García, Mixture model-based clustering and logistic regression for automatic detection of microaneurysms in retinal images, in: SPIE Medical Imaging, International Society for Optics and Photonics, 2009, pp. 72601M–72601M.
- [137] M.J. Cree, The Waikato Microaneurysm Detector, The University of Waikato, Technical Report.
- [138] B. Zhang, X. Wu, J. You, Q. Li, F. Karray, Hierarchical detection of red lesions in retinal images by multiscale correlation filtering, in: SPIE Medical Imaging, International Society for Optics and Photonics, 2009, pp. 72601L–72601L.
- [139] A. Mizutani, C. Muramatsu, Y. Hatanaka, S. Suemori, T. Hara, H. Fujita, Automated microaneurysm detection method based on double ring filter in retinal fundus images, in: SPIE Medical Imaging, International Society for Optics and Photonics, 2009, pp. 72601N–72601N.
- [140] C. Lobo, I. Pires, J. Cunha-Vaz, Diabetic macular edema, in: Optical Coherence Tomography, Springer, 2012, pp. 1–21.
- [141] R.P. Phillips, T. Spencer, P.G.B. Ross, P.F. Sharp, J.V. Forrester, Quantification of diabetic maculopathy by digital imaging of the fundus, *Eye* 5 (1) (1991) 130–137.
- [142] W. Zhang, K. Yamamoto, S. Hori, Optical coherence tomography for assessment of diabetic macular edema, *Int. J. Ophthalmol.* 1 (4) (2008) 370–373.
- [143] J. Nayak, P.S. Bhat, U.R. Acharya, Automatic identification of diabetic maculopathy stages using fundus images, *J. Med. Eng. Technol.* 33 (2) (2009) 119–129.
- [144] S.R. Sadda, O. Tan, A.C. Walsh, J.S. Schuman, R. Varma, D. Huang, Automated detection of clinically significant macular edema by grid scanning optical coherence tomography, *Ophthalmology* 113 (7) (2006), p. 1187-e1.
- [145] C. Strøm, B. Sander, N. Larsen, M. Larsen, H. Lund-Andersen, Diabetic macular edema assessed with optical coherence tomography and stereo fundus photography, *Invest. Ophthalmol. Visual Sci.* 43 (1) (2002) 241–245.
- [146] B.Y. Kim, S.D. Smith, P.K. Kaiser, Optical coherence tomographic patterns of diabetic macular edema, *Am. J. Ophthalmol.* 142 (3) (2006) 405–412.
- [147] H. Sánchez-Tocino, A. Alvarez-Vidal, M.J. Maldonado, J. Moreno-Montañés, A. García-Layana, Retinal thickness study with optical coherence tomography in patients with diabetes, *Invest. Ophthalmol. Visual Sci.* 43 (5) (2002) 1588–1594.
- [148] M.R. Hee, C.A. Puliafito, J.S. Duker, E. Reichel, J.G. Coker, J.R. Wilkins, J.S. Schuman, E.A. Swanson, J.G. Fujimoto, Topography of diabetic macular edema with optical coherence tomography, *Ophthalmology* 105 (2) (1998) 360–370.
- [149] A.S. Neubauer, C. Chryssafis, S.G. Priglinger, C. Haritoglou, M. Thiel, U. Welge-Lüßen, A. Kampik, M.W. Ulbig, Topography of diabetic macular oedema compared with fluorescein angiography, *Acta Ophthalmol. Scand.* 85 (1) (2007) 32–39.
- [150] R. Kohavi, G.H. John, Wrappers for feature subset selection, *Artif. Intell.* 97 (1) (1997) 273–324.
- [151] P. Langley, Selection of relevant features in machine learning, in: Proceedings of the AAAI Fall Symposium on Relevance, AAAI Press, 1994, pp. 140–144.
- [152] F. Aptel, P. Denis, F. Rouberol, C. Thivolet, Screening of diabetic retinopathy: effect of field number and mydriasis on sensitivity and specificity of digital fundus photography, *Diabetes Metab.* 34 (3) (2008) 290–293.
- [153] P. Kahai, K.R. Namuduri, H. Thompson, A decision support framework for automated screening of diabetic retinopathy, *Int. J. Biomed. Imaging*, 2006.
- [154] A. Osareh, M. Mirmehdı, B.T. Thomas, R. Markham, Classification and localisation of diabetic-related eye disease, in: Proceedings of the 7th European Conference on Computer Vision-Part IV, ECCV '02, 2002.
- [155] A.S. Neubauer, C. Chryssafis, M. Thiel, S. Priglinger, U. Welge-Luben, A. Kampik, Screening der diabetischen retinopathie und papillentopographie mit dem 'retinal thickness analyzer' (rta), *Der Ophthalmologe* 102 (2005) 251–258.
- [156] N. Larsen, J. Godt, M. Grunkin, H. Lund-Andersen, M. Larsen, Automated detection of diabetic retinopathy in a fundus photographic screening population, *Invest. Ophthalmol. Visual Sci.* 44 (2) (2003) 767–771.
- [157] C. Agurto, V. Murray, E. Barriga, S. Murillo, M. Pattichis, H. Davis, S. Russell, M. Abramoff, P. Soliz, Multiscale AM-FM methods for diabetic retinopathy lesion detection, *IEEE Trans. Med. Imaging* 29 (2) (2010) 502–512.
- [158] K. Noronha, U.R. Acharya, K.P. Nayak, S. Kamath, S.V. Bhandary, Decision support system for diabetic retinopathy using discrete wavelet transform, *Proc. Inst. Mech. Eng. H J. Eng. Med.* 227 (3) (2013) 251–261.
- [159] H.J. Jelinek, M.J. Cree, D. Worsley, A. Luckie, P. Nixon, An automated microaneurysm detector as a tool for identification of diabetic retinopathy in rural optometric practice, *Clin. Exp. Optom.* 89 (5) (2006) 299–305.
- [160] A.B. Hansen, N.V. Hartvig, M.S. Jensen, K. Borch-Johnsen, H. Lund-Andersen, M. Larsen, Diabetic retinopathy screening using digital non-mydratic fundus photography and automated image analysis, *Acta Ophthalmol. Scand.* 82 (6) (2004) 666–672.
- [161] M.D. Abràmoff, J.M. Reinhardt, S.R. Russell, J.C. Folk, V.B. Mahajan, M. Niemeijer, G. Quellec, Automated early detection of diabetic retinopathy, *Ophthalmology* 117 (6) (2010) 1147–1154.
- [162] B. Dupas, T. Walter, A. Erginay, R. Ordóñez, N. Deb-Joardar, P. Gain, J.C. Klein, P. Massin, Evaluation of automated fundus photograph analysis algorithms for detecting microaneurysms haemorrhages, and exudates, and of a computer-assisted diagnostic system for grading diabetic retinopathy, *Diabetes Metab.* 36 (0) (2010) 213–220.
- [163] S.C. Lee, E.T. Lee, Y. Wang, R. Klein, R.M. Kingsley, A. Warn, Computer classification of nonproliferative diabetic retinopathy, *Arch. Ophthalmol.* 123 (6) (2005) 759–764.
- [164] W.L. Yun, U.R. Acharya, Y.V. Venkatesh, C. Chee, L.C. Min, E.Y.K. Ng, Identification of different stages of diabetic retinopathy using retinal optical images, *Inf. Sci.* 178 (1) (2008) 106–121.
- [165] U.R. Acharya, E.Y.K. Ng, J.-H. Tan, S.V. Sree, K.-H. Ng, An integrated index for the identification of diabetic retinopathy stages using texture parameters, *J. Med. Syst.* 36 (2012) 2011–2020.
- [166] U.R. Acharya, K.C. Chua, E.Y.K. Ng, W. Yu, C. Chee, Application of higher order spectra for the identification of diabetes retinopathy stages, *J. Med. Syst.* 32 (2008) 481–488.
- [167] U.R. Acharya, C.M. Lim, E.Y.K. Ng, C. Chee, T. Tamura, Computer-based detection of diabetes retinopathy stages using digital fundus images, *Proc. Inst. Mech. Eng. H J. Eng. Med.* 223 (5) (2009) 545–553.
- [168] S. Lee, Y. Wang, Automatic retinal image quality assessment and enhancement, in: SHE Conference on Image Processing, vol. 3661, 2002, pp. 1581–1590.
- [169] Structured analysis of the retina, Accessed: 21/04/2013. URL <http://www.parl.clemson.edu/stare/>.
- [170] Digital retinal images for vessel extraction, Accessed: 21/04/2013. URL <http://www.isi.uu.nl/Research/Databases/DRIVE/>.
- [171] Diabetic retinopathy database calibration level 1, Accessed: 21/04/2013. URL <http://www2.it.lut.fi/project/imageret/diaretdb1/>.
- [172] P.M. Bossuyt, J.B. Reitsma, D.E. Bruns, C.A. Gatsonis, P.P. Glasziou, L.M. Irwig, J.G. Lijmer, D. Moher, D. Rennie, H.C.W. de Vet, Towards complete and accurate reporting of studies of diagnostic accuracy: the STARD initiative, *Br. Med. J.* 326 (7379) (2003) 41–44.
- [173] M.R.K. Mookiah, U.R. Acharya, C.M. Lim, A. Petznick, J.S. Suri, Data mining technique for automated diagnosis of glaucoma using higher order spectra and wavelet energy features, *Knowl. Based Syst.* 33 (2012) 73–82.
- [174] U.R. Acharya, O. Faust, S.V. Sree, D.N. Ghista, S. Dua, P. Joseph, V.I.T. Ahamed, N. Janarthanan, T. Tamura, An integrated diabetic index using heart rate variability signal features for diagnosis of diabetes, *Comput. Methods Biomed. Eng.* 16 (2) (2013) 222–234.

Muthu Rama Krishnan Mookiah is a Research Engineer in Ngee Ann Polytechnic, Singapore. He received his B.E. from Sethu Institute of Technology in 2002 and M.Tech. in Biomedical Signal Processing and Instrumentation from SASTRA

University in 2005 and Ph.D. from Indian Institute of Technology Kharagpur in 2012. He has published more than 25 papers in international journals and conferences. His major research interests are in Medical Image Analysis, and Pattern Classification.

U. Rajendra Acharya is a visiting faculty in biomedical engineering department at the Ngee Ann Polytechnic, Singapore. He is also adjunct professor at the University of Malaya, Malaysia, adjunct faculty at Singapore Institute of Technology—University of Glasgow, Singapore, and associate faculty at Singapore Institute of Management University, Singapore. He received his Ph.D. from National Institute of Technology Karnataka, Surathkal, India and D.Eng. from Chiba University, Japan. He has published more than 285 papers, including 178 papers in refereed international SCI-IF (Science Citation Index-Impact Factor) journals, as well as international conference proceedings (48), textbook chapters (62), and books (16). The h-index of his work in SCOPUS is 25 without self-citations. He has worked on various funded projects with grants worth more than 2 million SGD. He is an editorial board member of many journals, and has served as Guest Editor for numerous journals. His major interests are biomedical signal processing, bio-imaging, data mining, visualization and biophysics for improved healthcare design, delivery and therapy.

Chua Kuang Chua is a Senior Lecturer in Ngee Ann Polytechnic, Singapore. He received his B.Eng. (Hon) from National University of Singapore in 1989 and M.Sc. (Dist) in Audio System Engineering from University of Essex in 1997 and Ph.D. from Queensland University of Technology in 2010. He has published more than 20 papers in international journals and conferences. His major interests are in Biomedical Signal Processing, Digital Signal Processing, and Artificial Intelligence.

Lim Choo Min is a senior director in the school of Engineering, Ngee Ann Polytechnic, Singapore. He received the B.Eng., M.Eng., and Ph.D. degrees from the National University of Singapore in 1976, 1981 and 1986, respectively. He has published more than 80 international journal papers and edited a book. His research interests include neural network-based control, fuzzy logic control, bioinformatics, optimization and the development of hardware (training kit sets) and software for supporting mobile computing.

E.Y.K. Ng is an associate professor at the Nanyang Technological University in the School of Mechanical and Aerospace Engineering. He received Ph.D. at Cambridge University with a Cambridge Commonwealth Scholarship. His main area of research is thermal imaging, biomedical engineering; CFD/CHT. He Eddie is member of Singapore Biomedical Standards Committee, and an adjunct National University Hospital Scientist. He has published more than 400 papers in refereed international SCI journal (226); international conference proceedings (81), textbook chapters (82) and others (22). Eddie is Editor-in-Chief for the J. Mech. Med. Biol. and J. Med. Imaging Health Inf.; Strategy Association Editor-in-Chief for World J. Clin. Oncol; Association Editor for Int. J. Rotating Mach.; Comput. Fluid Dyn. J. (CFDJ); Int. J. Breast Cancer, Chin. J. Med., Open Med. Inf. J., Open Numer. Methods J., J. Healthcare Eng. and Guest Editor for various other journals. He is an invited keynote speaker for many International scientific conferences/workshops. He has co-edited 10 books on "Cardiac Pumping and Perfusion Engineering" by WSPC Press (2007); "Imaging and Modelling of Human Eye" by Artech House (2008); "Distributed Diagnosis and Home Healthcare, D2H2 v.1 & 3" by ASP (2009, 2012); "Performance Evaluation in Breast Imaging, Tumor Detection & Analysis" by ASP (2010); "Computational Analysis of Human eye with Applications" by WSPC (2011); "Multimodality Breast Cancer Imaging" by SPIE (2013); "Human eye imaging and modeling" & "Image Analysis and Modeling in Ophthalmology" & "Ophthalmology Imaging and Applications" by CRC (2012, 2013). Also, he co-authored a text book: "Compressor Instability with Integral Methods" by Springer (2007). More details are available upon request and in URL: <http://www.researcherid.com/rid/A-1375-2011>.

Augustinus Laude is Deputy Head of Research and Consultant Ophthalmologist at the National Healthcare Group Eye Institute, Singapore as well as adjunct Research Fellow at the Singapore Eye Research Institute (SERI). He graduated from the University of Edinburgh, United Kingdom in 1996 and furthered his interests by obtaining his Master of Science in Investigative Ophthalmology and Vision Science at the University of Manchester in United Kingdom in 2000 and Master of Medicine in Ophthalmology at the National University of Singapore in 2003. Subsequently, he obtained his fellowship with the Royal College of Surgeon in Edinburgh, United Kingdom and the Academy of Medicine, Singapore in 2008. The clinical interests of him include Vitreo-Retina, Cataract and General Ophthalmology.